

**Modeling and Development of Insulation Materials in Subsea
Pipelines**

Submitted by

Ibrahim Masaud Ahmed

A thesis submitted to

School of Graduate Studies in Partial Fulfillment of the

Requirements for the Degree of

Master of Mechanical Engineering

Faculty of Engineering and Applied Science Memorial University of

Newfoundland

May 2018

St. John's

Newfoundland

ABSTRACT

Flow assurance is a major issue in subsea pipelines that transport crude oil and gas. Thermal insulation is crucial in preventing and controlling the formation of hydrates, asphalt or wax that can block flowlines. Heavy components of crude oil begin to form as hydrates, asphalt and wax at low flow temperature. In addition, high pressure and low temperature start the formation of hydrates, asphalt and wax in gas pipelines. When the temperature of crude oil decreases due to increase in its viscosity in a flowline, this causes an increase in pump power consumption. This research includes analysis of heat loss, temperature profiles in steady state flows, and temperature profiles in transient flows of the startup mode for transporting crude oil in deep water pipelines. The research focuses on temperature profiles that use several thicknesses of materials. The methodology used is a Matlab program. Firstly, the program validates the results for the unchanging geometry and thermal properties of the materials, to investigate temperature profiles during the start-up of crude oil along the length of the pipeline. The calculation has achieved approximate results. Then the model uses new insulation materials, crude oil, temperature, inner diameter and outer diameter for the same length of the pipeline. Moreover, this research has investigated the cool down time for flow shutdown of crude oil in pipelines, which is a primary issue in the production of offshore oil and gas. Cool down time is considered for two cases, which are exposed insulation pipelines in seawater and insulated pipeline buried under seawater. The research uses ANSYS Fluent CFD for sample runs of the models to validate the Matlab program output. The ANSYS Fluent focuses on steady state and transient flow temperature profiles during crude oil start-up, and examines the effects of several insulation thicknesses and the low thermal conductivity of materials.

Keywords: cools down time, heat loss, hydrate, insulation materials, pipeline, steady state, temperature and transient.

ACKNOWLEDGEMENTS

I would like to convey many thanks to my supervisors, Dr. John Shirokoff and Dr. Aezeden Mohamed, for their support, motivation, encouragement, supervision and suggestions throughout my research. Their extensive guidance motivated me to complete my thesis successfully.

Also, I am very grateful to the Higher Institute of Technology of Tarhuna, Libya and Management Scholarships Libya for funding my study in Canada.

I would like to give great thanks to my mother, sisters and brothers, who have encouraged me to pursue this study.

CONTENTS

ABSTRACT	ii
ACKNOWLEDGEMENTS	iv
LIST OF TABLES	viii
LIST OF FIGURES	ix
Nomenclature.....	xiv
Greek symbols	xv
Subscript.....	xv
CHAPTER ONE: INTRODUCTION.....	1
1. Background.....	1
2. Scope and objective of study	2
3. Thesis Organization.....	3
CHAPTER TW: LITERATURE REVIEW	5
1. Design to Resist Outer Pressure	5
2. Design to Resist Inner Pressure	5
3. Pipelines Buried Under Water	7
4. Types of Thermal Insulation Materials	13
5. Phase Change Materials	20
6. Hydrates.....	21
7. Wax and Asphalt	23
8. Pipe-in-Pipe Insulation	24
9. Thermal Insulation of Subsea Oil and Gas Pipelines	26
9.1. Friction loss along pipelines	29
9.2. Temperature distribution along pipelines	29
9.3. The rate of heat loss.....	30

9.4. Overall heat transfer coefficient	30
9.5. Temperature distribution along pipelines	31
9.6. Temperature distribution at radius of insulation material	31
CHAPTER THREE: METHODOLOGY	32
1. Design.....	32
1.1. Some considerations for insulation	33
1.2. Insulation and heating process.....	33
2. Physical Model	34
2.1 Geometrical parameters of pipeline.....	35
2.2 Mathematical model for steady and transient flowline temperature	36
2.3 Governing equations.....	36
2.4 Heat transfer and temperature for steady-state fluid flow	38
2.5 Transient temperature during startup.....	39
2.6 Transient temperature through flow rate change.....	39
2.7 Convection.....	39
2.8 Internal heat transfer coefficient.....	40
2.9 External heat transfer coefficient.....	41
2.10 Heat transfer coefficient for fully buried pipeline	42
2.11 Overall heat transfer coefficient for unburied and buried pipelines.....	42
3. Geometric Modeling of ANSYS Fluent Computation Fluid Dynamic (CFD).....	43
4. Mesh Simulation Modeling	44
5. Setup	45
6. Heat Transfer Modeling in Fluent CFD	46
6.1 Energy transport equation.....	46
6.2 Governing Equation.....	47

CHAPTER FOUR: RESULTS AND DISCUSSION	48
1. Validation between Matlab Program and digitized graphs.	48
2. Mathematical Model by Matlab Program.....	54
3. Cool-Down Time during Shutdown Flowline	59
4. ANSYS Fluent (CFD)	65
CHAPTER FIVE: CONCLUSION	75
Future Work.....	76
REFERENCES	77

LIST OF TABLES

Table 1 Geometrical parameters of pipeline and insulation	36
Table 2 Thermal properties of materials.....	36
Table 3 Values of heat loss for insulation pipeline with three insulation materials and four thicknesses	59

LIST OF FIGURES

Fig. 1 Strengths in a pressurized pipeline.....	7
Fig. 2 Circumferential stress in a pipeline pressurized internally and externally	7
Fig. 3 Temperature distribution in clay around the pipeline with heat flux.....	9
Fig. 4 Temperature along the circumferential external surface of the pipeline.....	10
Fig. 5 Temperature distributions on the seabed with variation of thermal conductivity ratio.....	10
Fig. 6 Normalized temperature versus the thermal conductivity ratio.....	11
Fig. 7 Temperature on the external pipeline surface versus initial cover depth ratio...	12
Fig. 8 Cool-down curves of pipe wall for burial depth.	13
Fig. 9 Pictures of cylindrical (D z 15 mm, h z 25 mm) samples of monolithic silica aerogels (a) unmodified NFC and (b) surface-modified MA-NFC.....	15
Fig. 10 SEM Pictures of (a) unmodified NFC and (b) maleic anhydride (MA)modified NFC. Unmodified NFC and the MA-modified NFC as seen in (c) and (d), respectively.	15
Fig. 11 The effect of the concentration of unmodified NFC and MA-modified NFC (A) The overall density of the monolithic silica aerogel. (b) Diameters of the cylindrical samples of aerogel.....	16
Fig. 12 The effect of unmodified NFC and MA-modified (a) The elastic modulus of the aerogel (b) comparable stiffness.....	16
Fig. 13 Polyurethane gel before washing and drying steps (left) and aerogel counterpart after supercritical CO ₂ drying (right).	18

Fig. 14 Gelling time t_{gas} as a function of DABCO TMR concentration CDABCO TMR in the initial polyurethane sol.	18
Fig. 15 Mean thermal conductivity as a function of DABCO TMR concentration CDABCO TMR.	19
Fig. 16 Pictures of polyurethane sample (density = 0.12 g/cm^3) during uniaxial compression testing, and after stress relaxation.	19
Fig. 17 Stress-strain curves for polyurethane aerogels prepared from different CDABCO TMR leading to different mean bulk densities.	20
Fig. 18 Evolution of compressive modulus E as a function of bulk density with the estimated scaling law associated.	20
Fig. 19 Photograph of an actual hydrate block.	23
Fig. 20 Electrically Heated Pipe-in-Pipe	26
Fig. 21 Schematic of the pipe insulation system.	27
Fig. 22 Cool-down time of internal fluid with a single insulation layer of different materials.	28
Fig. 23 Cool-down time of internal fluid by combining aerogel insulation with paraffin wax or alumina oxide NPCM.	28
Fig. 24 The segment of a straight insulated pipeline.	35
Fig. 25 Sketch of simulation modeling.	44
Fig. 26 Mesh of pipeline.	45
Fig. 27 Run calculation of setup.	46
Fig. 28 Validation of transient flow temperature profile on the length of the steel pipeline between digitized graph and mathematical model for polyethylene insulation.	49

Fig. 29 Validation of steady state flow temperature profile on the length of the steel pipeline between digitized graph and mathematical model for polyethylene.	50
Fig. 30 Validation of transient flow temperature profile on the length of the steel pipeline between digitized graph and mathematical model for polypropylene insulation.	51
Fig. 31 Validation of steady state flow temperature profile on the length of the steel pipeline between digitized graph and mathematical model for polypropylene insulation.	52
Fig. 32 Validation of transient flow temperature profile on the length of the steel pipeline between digitized graph and mathematical model for polyurethane insulation.	53
Fig. 33 Validation of steady state flow temperature profile on the length of the steel pipeline between digitized graph and mathematical model for polyurethane insulation.	54
Fig. 34 Steady-state-flow temperature profiles on the length of the steel pipeline with polyurethane foam layers of various thicknesses.	55
Fig. 35 Transient flow temperature profiles on the length of the pipeline with a polyurethane foam layer of 2.54 cm.	56
Fig. 36 Steady-state-flow temperature profiles on the length of the steel pipeline with aerogel layers of various thicknesses.	56
Fig. 37 Transient flow temperature profiles on the length of the pipeline with an aerogel layer of 2.54 cm thick.	57
Fig. 38 Steady-state-flow temperature profiles on the length of the steel pipeline with polyurethane aerogel layers of various thicknesses.	58

Fig. 39 Transient flow temperature profiles on the length of the steel pipeline with a polyurethane aerogel layer of 2.54 cm.....	59
Fig. 40 Cool-down time temperature profiles during shutdown with several insulation thicknesses of polyurethane foam exposed pipeline in seawater.	60
Fig. 41 Cool-down time temperature profiles during shutdown with several insulation thicknesses of aerogel exposed pipeline in seawater.	61
Fig. 42 Cool-down time temperature profiles during shutdown with several insulation thicknesses of polyurethane aerogel exposed pipeline in seawater.	62
Fig. 43 Cool-down time temperature profiles during shutdown with several insulation thicknesses of polyurethane foam for pipeline buried under seawater..	63
Fig. 44 Cool-down time temperature profiles during shutdown with several insulation thicknesses of aerogel pipeline buried under seawater.	64
Fig. 45 Cool-down time temperature profiles during shutdown with several insulation thicknesses of polyurethane aerogel for pipeline buried under seawater.	65
Fig. 46 Validation between CFD and the mathematical model steady state temperature profiles on the length of pipeline subsea with several thicknesses of polyurethane foam.	66
Fig. 47 Validation between CFD and the mathematical model transient temperature profiles on the length of pipeline subsea thickness 2.54 cm of polyurethane foam.	67
Fig. 48 Validation between CFD and the mathematical model steady state temperature profiles on the length of pipeline subsea with several thicknesses of aerogel.	68
Fig. 49 Validation between CFD and the mathematical model transient temperature profiles on the length of subsea pipeline with thickness 2.54 cm of aerogel.	69

Fig. 50 Validation between CFD and the mathematical model steady state temperature profiles on the length of subsea pipeline with several thicknesses of polyurethane aerogel.....	72
Fig. 51 Validation between CFD and the mathematical model transient temperature profiles on the length of subsea pipeline thickness 2.54 cm of polyurethane aerogel.....	71
Fig. 52 (a, b, c, &d) The effect of several insulation thickness simulations on temperature distribution through layers of polyurethane foam on the radius of the pipeline.....	74
Fig. 53 (a, b, c, &d) The effect of several insulation thickness simulations on temperature distribution layers of aerogel on the radius of the pipeline.....	73
Fig. 54 (a, b, c, &d) The effect of several insulation thickness simulations on temperature distribution layers of polyurethane aerogel on the radius of the pipeline.....	74

Nomenclature

R_e	Reynolds number
N_u	Nusselt number
P_r	Prandtl number
V	Velocity of fluid, m/s
D	Diameter of pipeline, m
ν	Fluid kinematic viscosity
h	Heat transfer coefficient, $W/m^2 K$
f	Friction factor
L	Length of pipeline, m
g	Gravitational constant, m/s^2
T	Temperature of fluid, $^{\circ}C$
U	Overall heat transfer coefficient, $W/m^2 K$
t	Time, s
r	Radius of pipeline, m
A	Area of surface or section, m^2
k	Thermal conductivity, $W/m K$
C_p	Specific heat
\dot{m}	Mass flow rate, kg/s
m	Mass of fluid, kg
R	Thermal resistance, $^{\circ}C/W$
s	Thickness of insulation, m
a	Parameter group defined
b	Parameter defined

c	Parameter defined
q	Heat loss, J
$\partial T / \partial r$	The radial temperature gradient, °C/m
G	Thermal gradient outside the insulation, °C/m
z	Distance between top of soil and center of pipeline, m.

Greek symbols

μ	Dynamic viscosity, Kg/m s
α	Variable define
β	Variable defined
γ	Variable defined
ρ	Density of fluid, Kg/m ³
θ	Angle between the principal thermal gradient and pipe orientation, degrees

Subscript

i	Inlet, inner, initial
o	Outer
n	Number
p	Pressure
x	Location of length
f	Fluid
acc	Accumulation

CHAPTER ONE: INTRODUCTION

1. Background

The study of transient heat transfer in many layered complex pipelines with active heating is an essential aspect of flow assurance schemes and working strategies of deep water seabed pipelines that use pipe-in-pipe or sandwich methods. With increasing water depth and tie-back distance, pipeline insulation has become mandatory for all kinds of deep-water developments. For the subsea production of pipelines, active heating or chemical inhibitors are needed when passive thermal insulation is not enough to prevent wax deposition and hydrate formation that may occur during the warm-up or cool-down of pipelines [1]. Accurate analysis of transient heat transfer in complex pipelines is necessary to predict temperature progression along the pipeline, to control the temperature using the necessary amounts of chemical inhibitors or appropriate means of heating [1].

Extreme pressure and extreme temperature conditions in the flow carried through buried pipelines, when combined with imperfections in the bed of the trench along the pipe, present a potential situation for vertical upheaval and buckling. The uncertainties correlated with the parameters involved in the simultaneous pipe-soil uplift size and vertical driving force are widely recognized [2,3]. The use of polymer syntactic foams reinforced with glass micro balloons for pipeline insulation in deep water needs further consideration of its behaviour. For example, the foam layers are protected by a protective thermoplastic sheath on the developed structure; the effect of this protection has been studied using foam samples embedded in pure polymer [4]. Thermal design includes conjoint steady state and transient heat transfer analyses. In the steady state setup, the production oil temperature reduces as it flows along the pipeline, due to the

heat transfer through the pipe wall to the surrounding environment. The temperature profile throughout the whole pipeline structure should be higher than required in order to stop hydrate and wax formation during an average operation. This is determined from steady-state flow and heat transfer computations [5]. Numerous experiments have confirmed the need to understand the uplift resistance provided by soil cover for pipe buried in rough soils [6-10]. The wax may be dense enough to block the flowline if the pipeline is shutdown longer than the regular time. Consequently, the time between the pipeline closure and restart is the most critical time for pipeline flow assurance. Therefore protective coating and insulation materials are suggested to cover its external surface to decrease the heat loss and temperature drop [11].

Crude oil usually needs to be transported for long distances in offshore pipelines. The crude oil is frozen in the system due to heat transfer through the pipeline walls to the surrounding subsea. Temperature related transportation problems can occur if pipelines are not insulated; the temperature will drop quickly. This will lead to the precipitation of asphaltenes or paraffin wax and the buildup formation of hydrates [12]. A petroleum wax deposit consists of some crude oil, water, gums, resins, sand and asphaltenes, contingent on the nature of the crude oil, and is captured during the deposition procedure. Heat losses from crude oil pipelines transporting viscous crude oil can be calculated using the increasing viscosity of the crude oil. This is caused by the decrease in crude oil temperature which causes an increase in pump power consumption [13].

2. Scope and objective of study

This study has focused on the thermal insulation pipelines used for subsea crude oil transportation. The aim is to investigate temperature profiles along the length of the insulation pipeline system during the start-up and flow shutdown periods. Several

cases of steady state temperature profiles during start-up are examined, along with two transient temperature profiles during the start-up and shutdown of flowlines. Additionally, heat loss is calculated for the period of the start-up of flowlines. This research includes the following steps:

- Firstly, the mathematical model is employed, using geometry, insulation materials, and properties of the fluid to investigate output. Then a new model is generated with a changed diameter, fluid properties, thermal insulation materials, internal temperature and ambient temperature for the same length of pipeline.
- Secondly, the cool down time for exposed pipeline in seawater and buried pipeline under seawater is calculated.
- Thirdly, using ANSYS (CFD) simulation, samples of insulation pipeline are simulated with four cases (thicknesses) and three thermal insulation materials, which are polyurethane foam, aerogel, and polyurethane aerogel. The results from mathematical and ANSYS (CFD) simulation are compared and validated.

3. Thesis Organization

Chapter 2 is a literature review of a design to resist outer and inner pressure for subsea pipelines and pipelines buried under water, types of thermal insulation materials, phase change material, hydrate formation during shutdown in flowlines, wax and asphalt existing in flowlines with a low temperature and high viscosity of oil, pipe in pipe insulation using electric heat pipelines, energy storage using phase change material for thermal insulation of pipe-in-pipe, friction loss and the rate of heat loss in pipelines.

Chapter 3 examines physical and mathematical models for the design of pipelines with high pressure and high temperature in seabed, some considerations of insulation and the heating process, physical and mathematical models for steady and transient

flowline temperatures, governing equations, heat transfer and temperature for steady state fluid flow, transient temperature through start-up, transient temperature through flow rate change, a heat transfer coefficient for internal and external fluid, a heat transfer coefficient for a fully buried pipeline, an overall heat transfer coefficient for a fully buried pipeline, geometric modeling of ANSYS Fluent CFD, mesh simulation modeling, heat transfer modeling in Fluent CFD, and an energy transport equation and governing equation for convection and conduction.

Chapter 4 conveys the results and discussion, the validation of mathematical model graphs digitized from published research [50], a mathematical model using Matlab program for steady state flow and transient flow temperature profiles during the start-up of flowlines, the cool-down time during shutdown of a flowline that runs in exposed insulation pipeline in seawater and in buried insulation pipeline under seawater. ANSYS Fluent (CFD) is used to validate results of the mathematical model, which consist of steady state and transient temperature profiles during the start-up for crude oil in an offshore pipeline, and simulation temperature distribution at the radius of insulation pipeline as it is decreased by low thermal conductivity and increased thickness of insulation materials. Chapter 5 is the thesis conclusion and future work.

CHAPTER TWO: LITERATURE REVIEW

1. Design to Resist Outer Pressure

Underwater pipelines that carry oil and gas are affected by pressure. A great outer pressure tends to cause the pipeline cross section to change to an oval shape and to break down. A fully round pipeline loaded by steadily increasing internal pressure would stay circular until the pressure reached the elastic critical pressure (PECR) as presented by following equation [14].

$$P_{\text{ecr}} = E/4 \left(\frac{R}{T} \right)^3 (1 - \nu^2) \quad (1)$$

The pipeline would then quickly collapse. For most marine pipelines, the elastic critical pressure is very high. For example, 30 inches of pipeline with a wall thickness of 22.2 mm has a flexible critical pressure of 12.5 MPa, identical to a water depth of 1,250 m, which would generate a collar strain of about 208 MPa [14]. Circumferential pressure output is potential, but flexible collapse happens first, except for quite thick pipelines. In addition, some pipelines are not quite circular to begin with and are not round to some extent. When an out-of-round pipeline is subjected to increased outer pressure, the out of roundness gradually increases, and becomes quite great as the pressure specified by equation 1 is approached [14].

2. Design to Resist Inner Pressure

Inner pressure from the included fluid is the most important loading a pipeline should carry. It is easy to forget how large the strengths generated by pressure are. Fig 1a is a cross-section of a model large-diameter gas pipeline of 30 inches that has an inner pressure of 15 MPa. If we want to determine the strength that the inner pressure pushes in the pipe wall, then we review the equilibrium of everything below the sectioning plane drawn in Fig 1a. Half of the pipe and half of the contents are redrawn in Fig 1b as a free body diagram. Then half of the pipe and half of the contents are

redrawn in Fig 1b as a free body diagram. The downward compression on a 1 m length of this system is the pressure of the gas multiplied by the area over which the pressure acts, a rectangle 0.75 m wide and 1 m long. Pulling upward on the same 1 m length is the tension in the pipe walls. There are no other vertical forces in a straight section of pipe. Since the system is in equilibrium, the stress in the pipe walls must be

$$(15 \text{ MPa}) \times (0.75 \text{ m}^2) = 11.25 \text{ MN}.$$

The hoop strain generated by internal pressure is statically determined, thus no important stress redistribution can happen and the strain is not modified or relieved by plasticity. If the hoop strain is too large the pipeline can yield circumferentially, and continued yielding will lead to thinning of the pipe wall and ultimately to a rupture. In terms of stress rather than strength, the hoop stress can be calculated from the equilibrium by essentially the same argument put into algebraic terms. Considering a pipeline with outer diameter d_o , inner diameter d_i , wall thickness S , inner pressure p_i , and outer pressure p_o , Fig 2a presents a cross section of this situation [14]. The pipeline is typically installed in a stress-free condition, separately from remaining stresses that have accumulated during the construction and installation process. As the hot fluid is pumped through the pipeline, the pipe unit will experience both thermal expansion and pressure induced stresses [8].

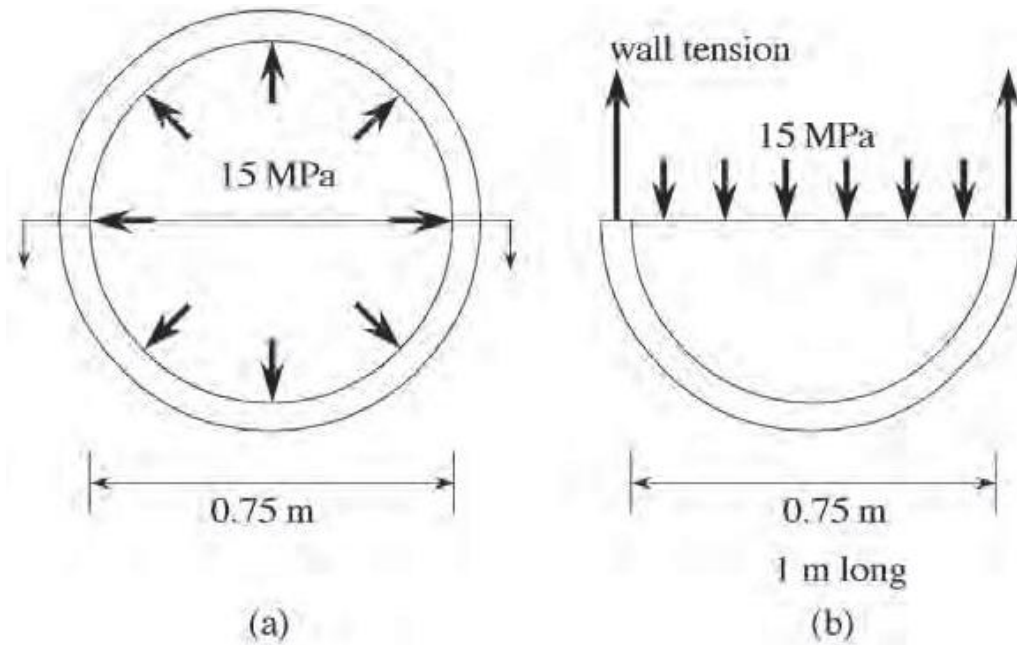


Fig. 1 Strengths in a pressurized pipeline [14].

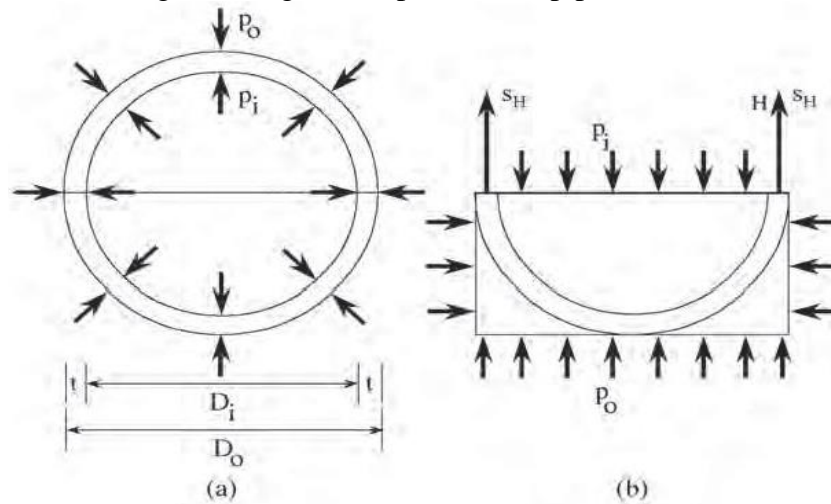


Fig. 2 Circumferential stress in a pipeline pressurized internally and externally [14].

3. Pipelines Buried Under Water

Subsea pipelines are frequently buried to keep the pipeline from external loads or to decrease heat losses. But, if the deepness of soil cover above the pipeline is not sufficient, in time the pipe can buckle upwards to reduce thermal strains [15]. Subsea pipelines are typically buried to prevent damage from fishing activities and to keep thermal insulation [16]. Flexible subsea pipelines used for oil and gas carrying are typically buried to sidestep damage from fishing activities and to supply thermal

insulation [17]. Pipeline burial is widespread in shallow water, which is fundamental to provide protection against outside loads such as fishing equipment. There are many types of trenching and backfill techniques ready made for submarine pipelines. In deeper water, the use of surface-towed gear is much more difficult due to the control of the catenary of the heavy tow wire and umbilical control. So, the use of a remote operated vehicles (ROV) based jetting system has proven more practical and economical for deeper water applications (>1000m) [18]. The great depth pipelines are prepared to deliver a mixture of crude and gas. Using a robotic ditch tool, pipelines are buried to increase the thermal insulation [19,5]. The subsea sand is a perfect thermal insulation, but the stone waste might supply little insulation. Therefore, the fluid runs between stones and causes a convection heat transfer. The buried pipelines reduce the heat transfer over the subsea and safely increase the pipeline cool down time [20]. The modeling of a buried pipeline must then consider the topology of a layered subsea and the thermal conductivity of the backfill material. A quantitative parametric investigation has evaluated the factors that affect the thermal field on a buried pipeline. It includes the examination of the outcome of the thermal power, the thermal properties of the backfill, the layer depth and the pipe diameter. It shows the thermal insulation has the efficiency of different materials; the pipeline buried in seabed transports mixtures of oil and gas and their associated impurities. These impurities have been sensitive to temperature and pressure, and are consequently deposited and accumulate under different conditions. The minimum required heat flux, 55 W/m^2 , was screened out for the pipes without insulation treatment. Fig. 3 presents the temperature distribution in the surrounding soil. The white space visible in Fig. 3 illustrates null value zones where temperature is not estimated in order to avoid numerical singularity issues [19].

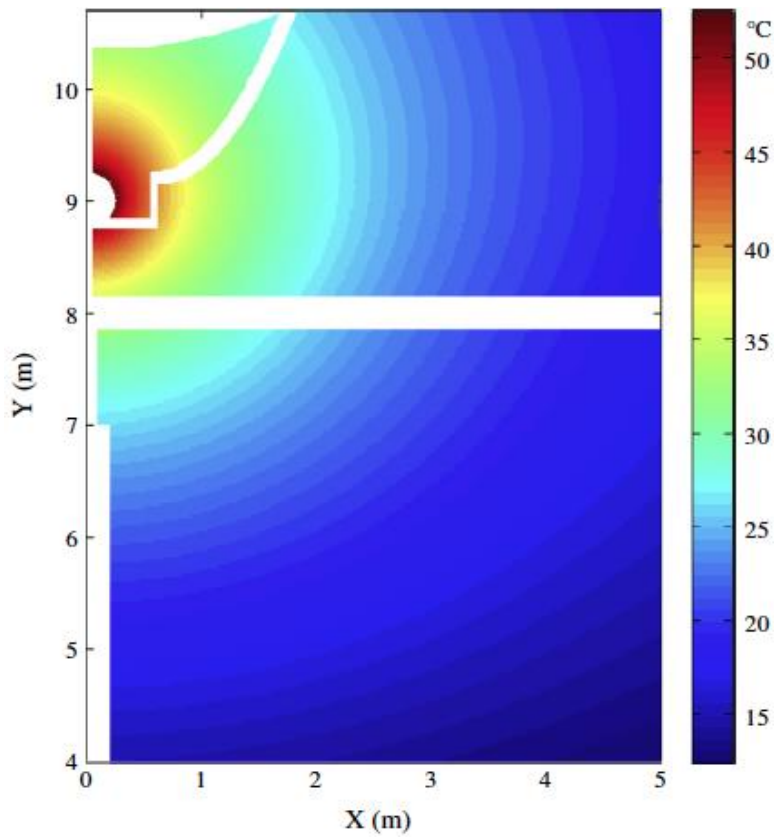


Fig. 3 Temperature distribution in clay around the pipeline with heat flux [19]

The moisture and an invalid ratio can change the thermal conductivity of clay, and the thermal conductivity of backfill changes during the consolidation process. The effect of the conductivity ratio between the backfill clay and the undisturbed top layer clay is studied. The thermal power loss is under 80 W/m and the temperature along the circumferential external surface of the pipeline is shown in Fig. 3 [19].

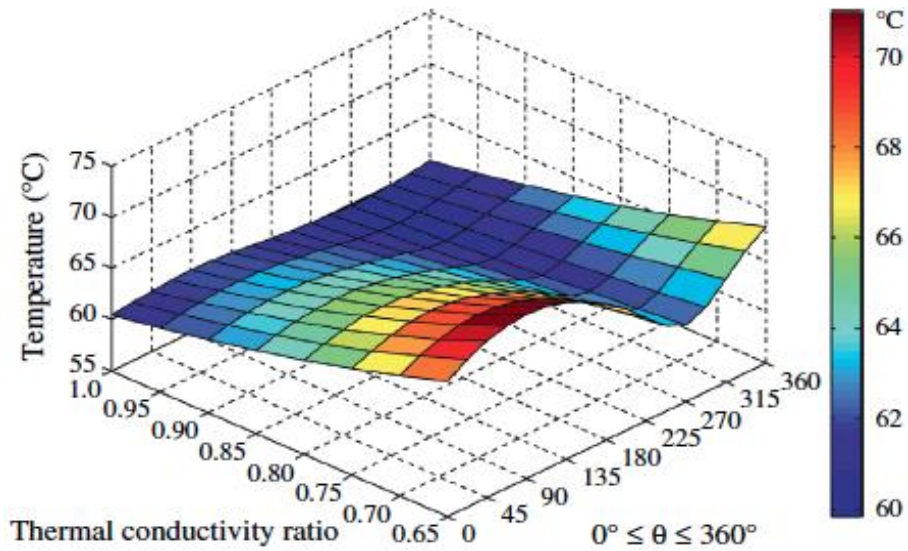


Fig. 4 Temperature along the circumferential external surface of the pipeline [8]

Fig. 5 presents temperature distributions in the subsea. The horizontal distance far from the centerline of the pipeline is normalized by the pipeline external diameter [19].

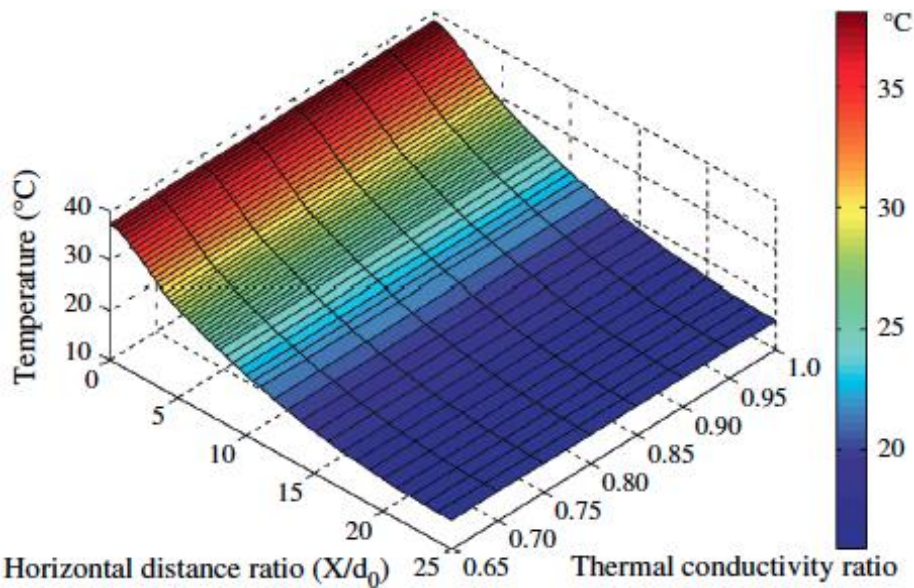


Fig. 5 Temperature distributions on the seabed with variation of thermal conductivity ratio [19]

To estimate the impact of the conductivity difference on the outside pipe wall and on the seabed temperature, Fig. 6 is shown with a temperature ratio normalized by the identical temperature for a conductivity ratio of 1. It should be noted that neglecting

the trenching and backfill effects results in increasing the temperature difference between the upper part and the minimum part of the pipeline. Backfill can decrease this difference [19].

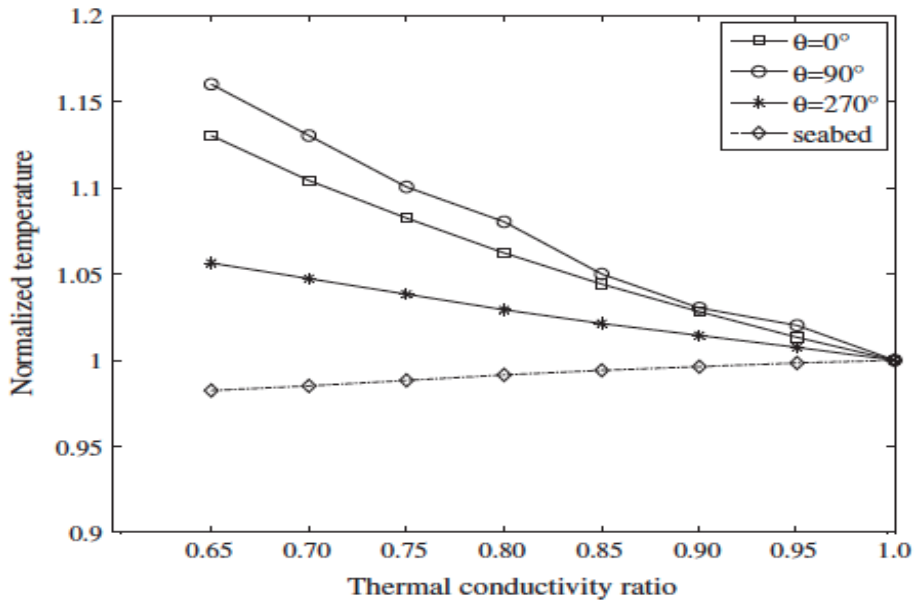


Fig. 6 Normalized temperature versus the thermal conductivity ratio [19]

Since thermal properties of backfill affect the fluctuation of temperatures on the outer surface, as discussed above, the impact of backfill on temperature distributions is further inspected with respect to cover depth. Under various cover depth cases, the temperature distribution along the circumferential surface to the pipeline is seen in Fig. 7 [19].

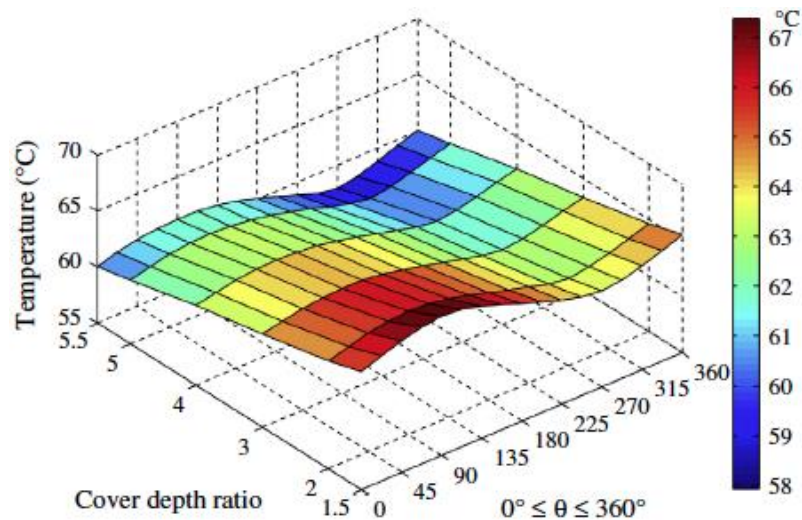


Fig. 7 Temperature on the external pipeline surface versus initial cover depth ratios [19]

High pressure and high temperature conditions (HPHT) in the oil transported over buried pipelines, when combined with imperfections at the bed of the trench along the pipe profile provide a possible scenario for vertical or upheaval (vertical) buckling. The uncertainties associated with the parameters involved in both pipe soil rise ability and vertical driving force are widely recognized [2]. Buried pipelines have been used in recent years as an economical and effective method to achieve thermal insulation. The benefits of buried and coated pipelines are compared to pipe-in-pipe systems including potential cost savings, an increase in allowable transient shut-down times and the longer duration of wax appearance and hydrate formation [18]. There is an agreement between the numerical modeling and the experimental modeling (see Fig. 8) that are focused on the heat loss mechanism of buried pipelines under water by semi-infinite porous average. The soil preparation, burying the pipe and trenching are challenging and time consuming tasks for these tests [21].

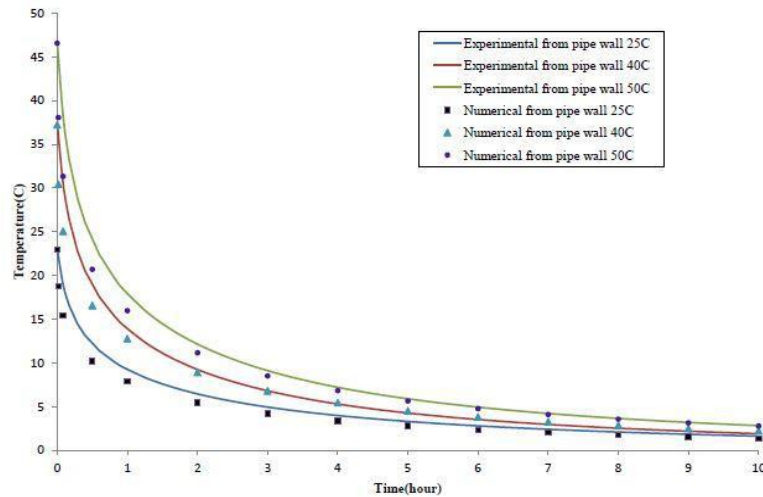


Fig. 8 Cool-down curves of pipe wall for burial depth [21].

4. Types of Thermal Insulation Materials

Blown foam materials give the best insulation properties. However, the foam is used to limit of deep water for exposed pipelines. Syntactic and combined syntactic foams have the best water depth ability because they offer the best insulation and hydrostatically strong properties, which offer strong mechanical properties that work well in very deep water. Thus, these materials do not have low thermal conductivity as needed [4]. The silica aerogel is associated with an organic polymer that is an active technique to overcome their weakness and to increase strengthening of the mechanical properties. Also, it includes an adjusting, which regulates the nanoskeleton of silica aerogel and utilizes various parts of the silica. This can lead to improved mechanical properties, mesoporosity and thermal conductivity. Dissimilar fortified silica aerogels have a density extent from 0.13 to 0.39 g/cm³. Compression forces from 11 to 400 kPa and a thermal conductivity of 0.039 W/m K [22] have been gained. The silica aerogel combination is made from dispersing nano fibrillated cellulose (NFC) into polydimethylsiloxane. Experiments to further improve the dispersing of the nano fibrillated cellulose in ethanol are made utilizing maleic anhydride as the flatten adjust

factor. The nano composites with nano fibrillated cellulose behave to improve the mechanical properties of silica aerogels, when thermal conductivity decreases just a little. Pictures of dried NFC reinforced silica aerogel composites and dried MA-modified NFC reinforced silica aerogel composites containing varying concentrations of NFC are presented in Fig. 9a and Fig. 9b, respectively. Fig. 10a and 10b display model pictures taken from the unmodified and MA- adjusted NFC, respectively, after they are dispersed in ethanol and then freeze dried. Scanning electron microscopy (SEM) pictures from fractured cross-sectional areas of silica aerogel composites made using unmodified and MA-modified NFC are seen in Fig. 10c and d, respectively. Fig. 12a clarifies how the final densities of dried NFC reinforced silica aerogel composites vary more linearly with the concentration than does the unmodified NFC. In expression of linear shrinkage of the aerogels during processing due to aging and to drying, the existence of the NFC has small but measurable effects, as seen in Fig. 12b. The elastic modulus E and the silica aerogel-based composite materials, as a function of NFC concentration, are offered in Fig. 12a. To estimate the influence of density on the flexible modulus of the composite materials, the E values of the NFC fortified silica aerogel composites are replotted in Fig. 12b with respect to density [23].

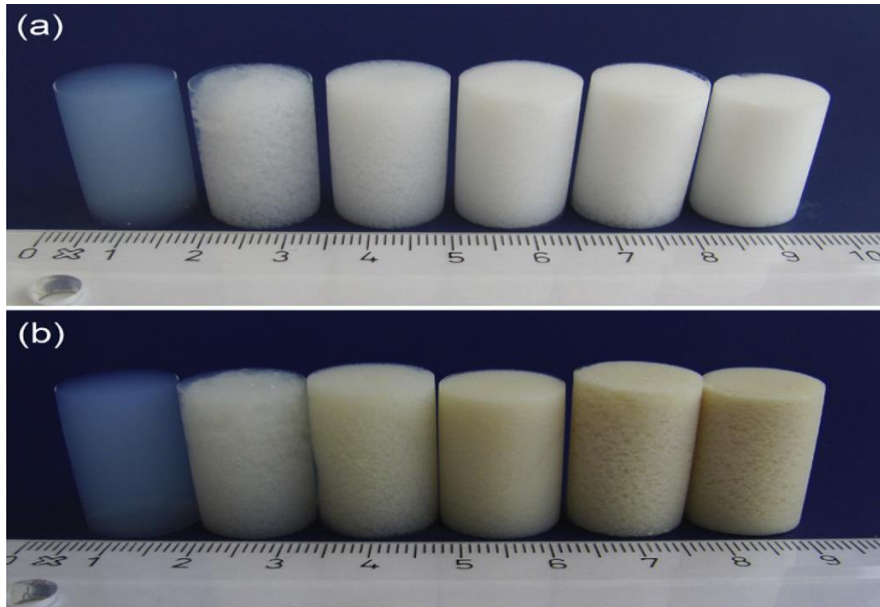


Fig. 9 images of cylindrical ($D \approx 15$ mm, $h \approx 25$ mm) samples of monolithic silica aerogels (a) unmodified NFC and (b) surface-modified MA-NFC [23].

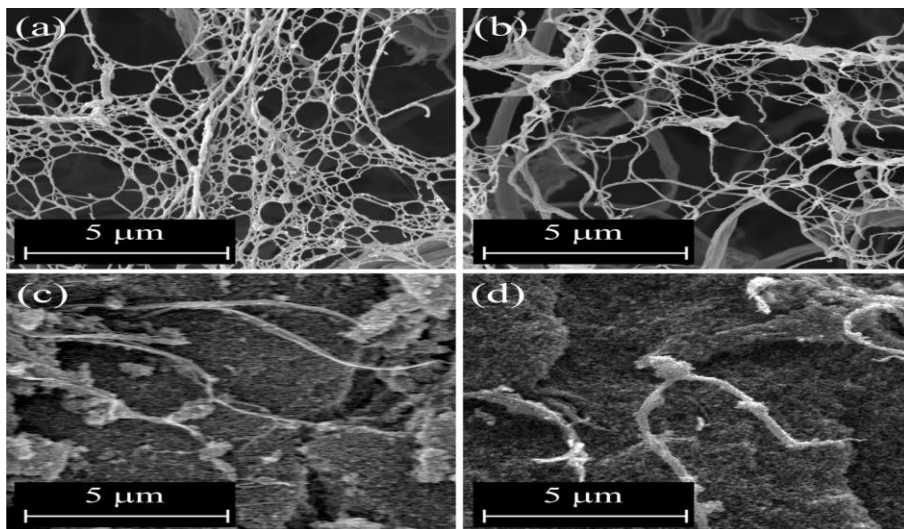


Fig. 10 SEM images of (a) unmodified NFC and (b) maleic anhydride (MA)-modified NFC. Unmodified NFC and the MA-modified NFC as seen in (c) and (d), respectively [23].

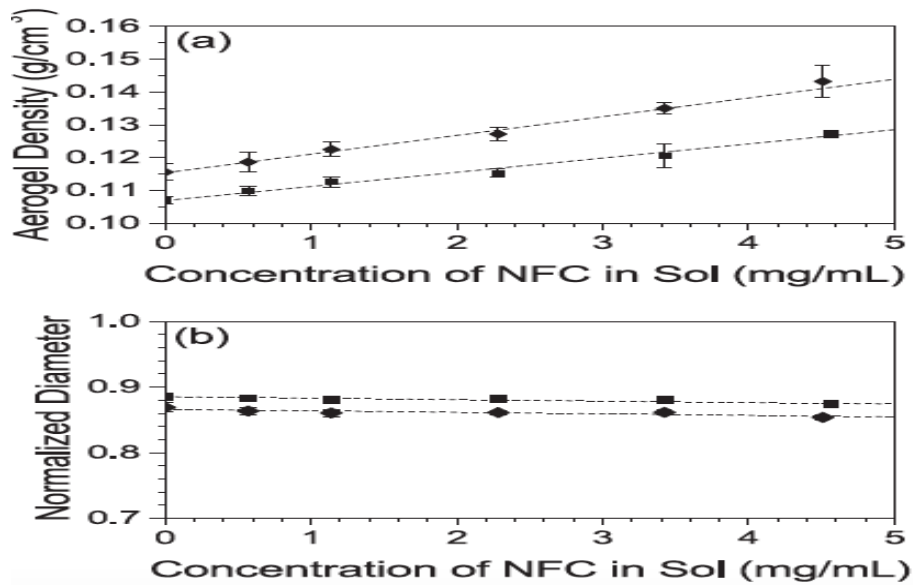


Fig. 11 The effect of the concentration of unmodified NFC and MA-modified NFC (a) The overall density of the monolithic silica aerogel. (b) Diameters of the cylindrical samples of aerogel [23].

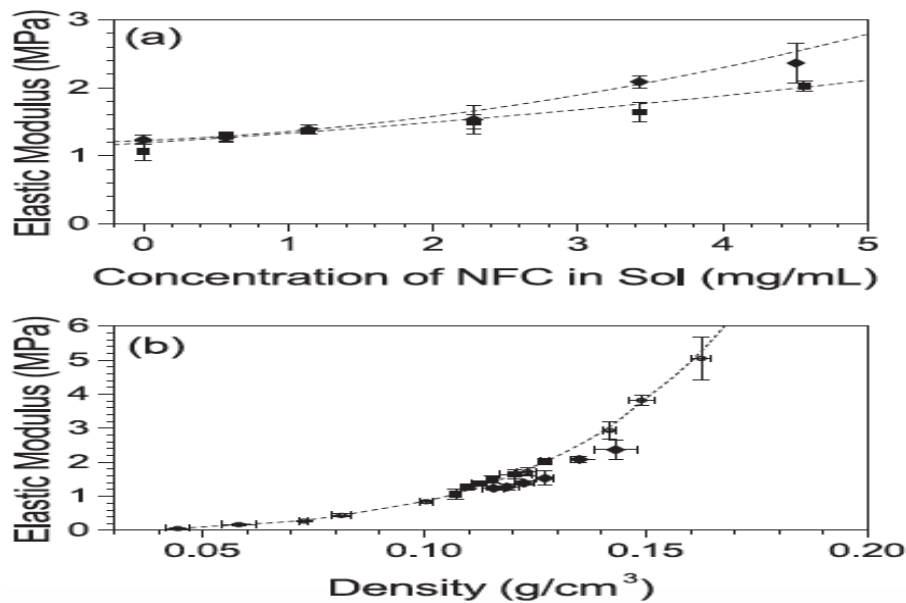


Fig. 12 The effect of unmodified NFC and MA-modified (a) The elastic modulus of the aerogel (b) comparable stiffness [23].

Polyurethane aerogel synthesis has improved thermal conductivity and mechanical properties. The lowering catalyst concentration first allows for a significant decrease in the kinetic reaction characterized with the gelation time. This parameter usually affects the texture polyurethane samples, with a considerable modification of bulk density,

porosity, and pore size distribution. The polyurethane aerogel offers thermal conductivity as low 0.017W/m K, able to withstand high pressure without breakage, and its compressive modulus reaches 7.8 MPa. At the termination of the synthesis process, the obtained monolithic polyurethane aerogels macroscopically appear opaque and white, as seen in Fig. 13. In a relatively traditional method, it has been observed in Fig. 14 that the gelling time t_g clearly builds on the first concentration of the polyurethane (Abbreviated in CDABCOTMR subsequently). Thermal conductivity evaluated in room situations is between 0.016 and 0.025 W/m K ± 0.001 for polyurethane aerogels synthesized with CDABCO TMR differing between 2.7 and 17.7 m/mole 1. Data given in Fig. 15 identify mean thermal conductivity standards. Uniaxial compression experiments are carried out on polyurethane models, with at least two models for each catalyst concentration scale. This organic aerogel displays a plastic distortion behaviour. The height of the sample can decrease to a high distortion scale (image c), and this deformation is fundamentally irreversible (image d), as appears in Fig. 16. The stress strain curves acquired from the compression experiments for some CDABCO TMR values cover the whole catalyst focus range as shown in Fig. 17. They offer two main distortion behaviours. Considering the effect of CDABCO TMR on bulk the density of polyurethane aerogels, a clear development of mechanical characteristics with sample density can be observed. In the situation of these polyurethane aerogels, a clear direction is observed between compressive modulus and bulk density, as shown in Fig. 18 [24].

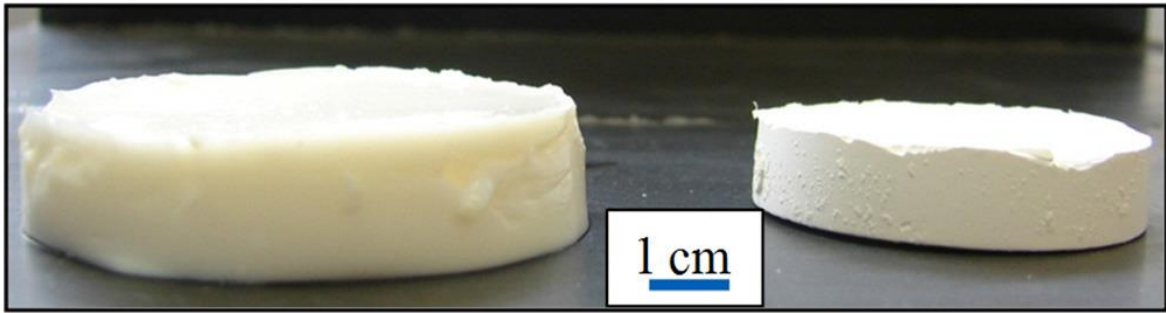


Fig. 13 Polyurethane gel before washing and drying steps (left) and aerogel counterpart after supercritical drying (right) [24].

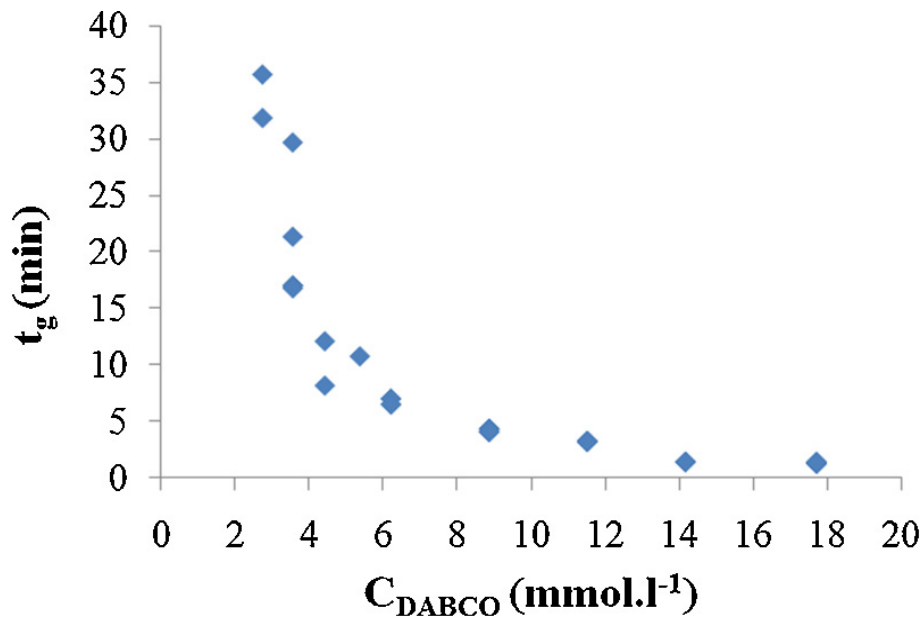


Fig. 14 Gelling time t_g as a function of DABCO TMR concentration $C_{\text{DABCO TMR}}$ in the initial polyurethane sol [24].

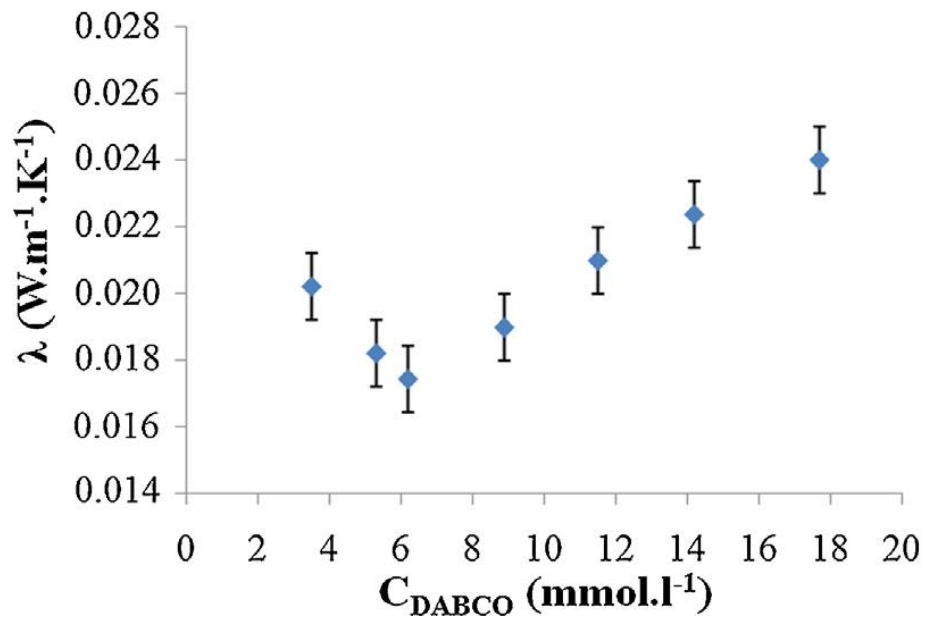


Fig. 15 Mean thermal conductivity as a function of DABCO TMR concentration C_{DABCO} [24].

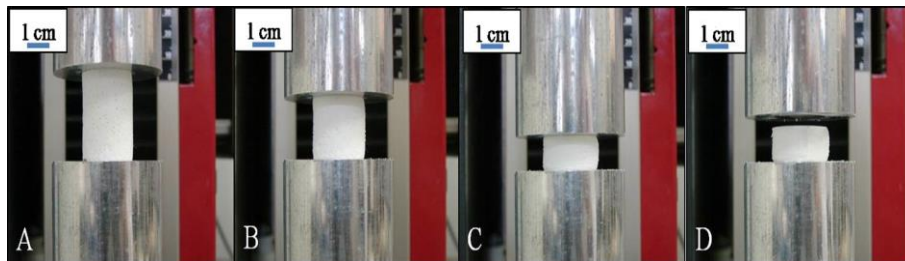


Fig. 16 Pictures of polyurethane sample (density = 0.12 g/cm³) during uniaxial compression testing and after stress relaxation [24].

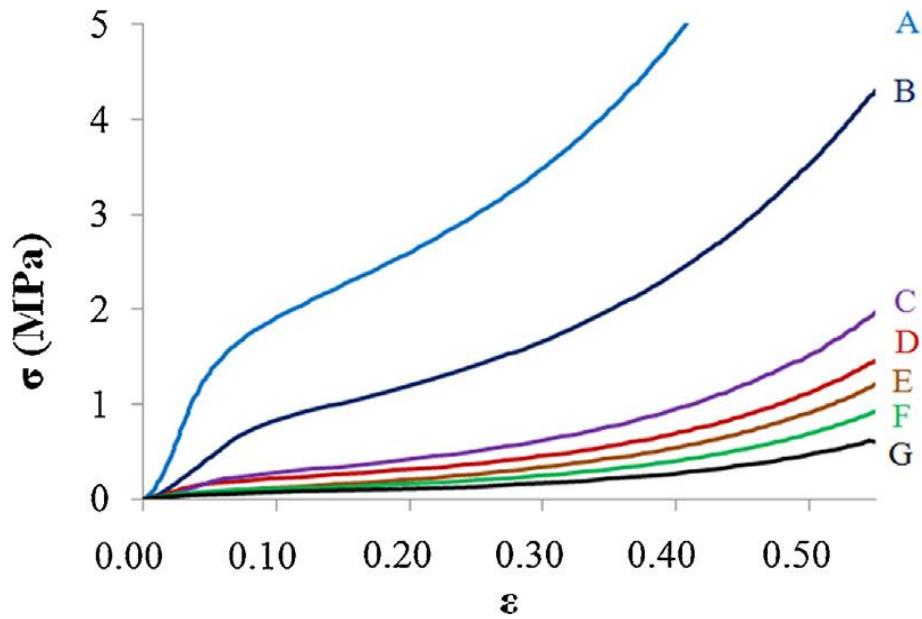


Fig. 17 Stress-strain curves for polyurethane aerogels prepared from different CDABCO TMR leading to different mean bulk densities [24].

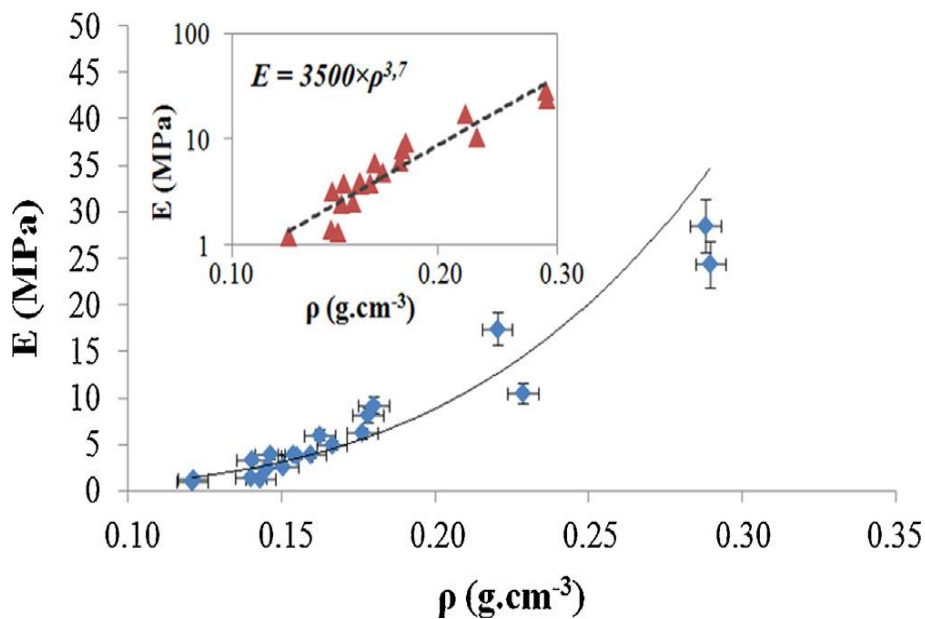


Fig. 18 Evolution of compressive modulus function of bulk density with the estimated scaling law associated [24].

5. Phase Change Materials

Paraffin wax is made on microcapsules consisting of pulp with a fusion temperature of around 42°C and with melamine-formaldehyde and resin synthesized utilizing in situ polymerization. Microcapsules are consistent with a globular style and a medium diameter of around 1.5 μm. Stable form phase change materials (PCM) built

on high density polyethylene blended with micro-encapsulated paraffin wax are prepared and inspected for implementation in thermal energy. The distribution of the capsules, including the high density polyethylene, was regular without either slope moving toward mass. The microencapsulated paraffin wax has high-latent heat material, whereas the high-density polyethylene matrix includes the consolidated form, constitutional denseness and the mechanical force of the last PCM. The frequent temperature method is used to define thermal conductivity and the heat allowance of the phase change materials. A hot plate unit is carefully utilized to define the latent heat of phase change materials. The thermal conductivity to allow for the inspected PCMs “decreased as the microcapsule content increased”. The latent, sensible heat and total heat of the PCMs “increased with the paraffin content” [25,26]. Phase change material (PCM) improved form stability by fertilization of hydrated to extensive graphite that was then plated with paraffin wax. Compound PCM has perfect thermal stabilization in the active temperature range from 25 to 50°C. Compound phase change material (PCM) has a high thermal conductivity of 3.643W/m K, has great latent heat, and perfect thermal reliability. Composite PCM is perfect for low temperature work due to its being favorable “for low temperature thermal energy storage” use [27].

6. Hydrates

Natural gas hydrates are crystal complexes established by the physical collection of water molecules and hydrocarbon liquids such as methane, ethane, propane, nitrogen, carbon dioxide and hydrogen sulphide. Hydrates are simply created when the hydrocarbon gas contains water at a high pressure and comparatively low temperature [28]. Hydrates might seem common in an offshore system of natural gas, water and appropriate temperature and compression. When the depth of water is more than 1000 m, the temperature deviations can be extremely small and water temperature

at the subsea reaches approximately 8°C [29]. Hydrates should be kept away from the offshore engineering equipment to prevent flow blockage (Fig. 19) in pipelines and seabed equipment [30]. Hydrates are of significance in deep water gas because ambient temperatures are the least sufficient to be in the hydrate compound zone at operative compression [28,31]. During shutdown, the pipeline temperature would be reduced due to heat transfer from the system to the environment's water. The insulation system of the pipeline is designed to save the temperature of liquid over the hydrate separation temperature until it stops separating. When the flow line system needs to keep out of the hydrate region and shut down time is longer than the cool down period, flow line depressurization may be an option. The transient simulation of this case is presented for along the pipeline and fluid carryover during blow down, as well as indicating if the target pressure to avoid hydrate formation can be reached [32]. Hydrate construction is a substantial problem in deep water processes and subsea pipeline in petroleum transportation, where process conditions are within the hydrate stability area. In those positions, when hydrate plugs are created, the formation of solid deposits was controlled. Four fundamental elements are required for hydrate creation: hydrate creating gases or water, low temperatures, and moderate to high pressures. Hydrate formation can be limited by governing one or more of these four elements, specifically water elimination from the fluid stream, heating and insulation of pipelines, depressurization, and acceptance of hydrate inhibitors [33, 28].



Fig. 19 Image of an actual hydrate block [30].

7. Wax and Asphalt

Wax in offshore flowlines poses many working problems, and has been considered by some authors [34-40]. Paraffin waxes are natural alkane complexes that are normally present in oil. At low temperature, these complexes can come out of the oil and form extended crystals. When the control of wax precipitation is not efficient, the waxy precipitate is able to increase and this is the reason for the disruption of production and the decrease of throughput, which will continue until full stoppage of the liquid line. Subsea production is easy, and pipelines are extremely receptive to wax precipitate and asphalt residues induced by the low temperature and pressure drop environment [39,40].

Asphalt is a compound fluid in crude oil and coal. Asphalt can be flocculate and shape precipitation under raised shear, high speed liquid conditions. Asphalt is insoluble in nonpolar solvents, but soluble in toluene or other aromatics setup solvents. Asphalt precipitations are extremely difficult to remove once they occur. For different wax precipitation and gas hydrates, asphalt formation is not simple. Repeated

asphalting precipitation occurs with wax precipitation, and makes the compound precipitations extremely arduous, viscous, and complicated to remove [40]. Wax sedimentation in crude oil pipelines can be economically destructive to petroleum companies. A technique used for wax sedimentation is sonic chemo metrics, which has been suitable for online valuation of wax sedimentation thickness in single-phase petroleum flow pipelines built on piggy back investigations. The first experiments were carried out to explore the prospect of stratifying this auditory chemo metric mechanism. The tests for a varied stream average need to be refined with another mechanism to improve “a model of predicting the wax deposition thickness under” different stream averages [41,42].

8. Pipe-in-Pipe Insulation

Pipe-in-pipe (PIP) system is used in many cases, which are considered over conventional single pipe systems. For example, production oil from high temperature reservoirs in deep water needs pipe-in-pipe insulation materials to fill the space between pipes by using insulation such as foam, granular, gel, and rigid gas or gaps [43].

Sylvain Denniel. et al. [44], report that companies have decided to improve the efficiency of the second level of the innovative technology of electrical heat effect as a solution for active heating of seabed pipelines within electrically heated (EH) pipe-in-pipe. This is in response to the “production challenges” of oil tanks with high flow assurance constraint “wax, gel and critical hydrate appearance temperatures”.

The work performed responds to the specific uncertainties associated with the drawing, invention, installation and procedure of an EH-PIP. The survey has confirmed that an EH-PIP is completely reliable and able to be constructed as a complex with minimum deviation from a natural PIP construction table, without impact on the

critical path. Moreover, “full scale” and laboratory testing have confirmed the heat tracing system to be fit for the aim of long term application in rising temperature applications. The survey has also allowed CFD thermal modeling techniques to be completely validated for future field analysis. The computational fluid dynamic (CFD) sample was therefore used to best recognize temperature distributions and to analyze compound heating operations. The thermal efficiency has confirmed that EH-PIP uses the cable heat with high efficiency, maximizing heat transfer to the pipeline and reducing heat loss to the sea, performing with an overall efficiency of circa 90%. Testing and analysis has shown that, even when degraded, one wire can be used to uniformly heat the contents of the pipeline during active operation. This means every wire installed on the pipe, in addition to the initial one, results in an extra 100% of increase and a complete 300% increase for the set of 4 wires as per the tested design. This, in combination with the experimental test outcome, leads to the conclusion that PIP is a reliable and more effective heating solution for complicated seabed tie backs in terms of procedure, economic value, and the ambience. A common characterization of the EH-PIP is that it is a standard reelable PIP process. Technip has added an effective heating process, which is located between the streamline walls with the insulation material for best performance. This system includes scale components, which contain the efficient insulation material aerogel, and structurally includes holes to adjust transit of cables. However, in the trace heating method, shown in Fig. 20, the heat power is supplied by pure joule resistive impact. The seabed power is supplying configuration, which includes a power umbilical and seabed connectors.

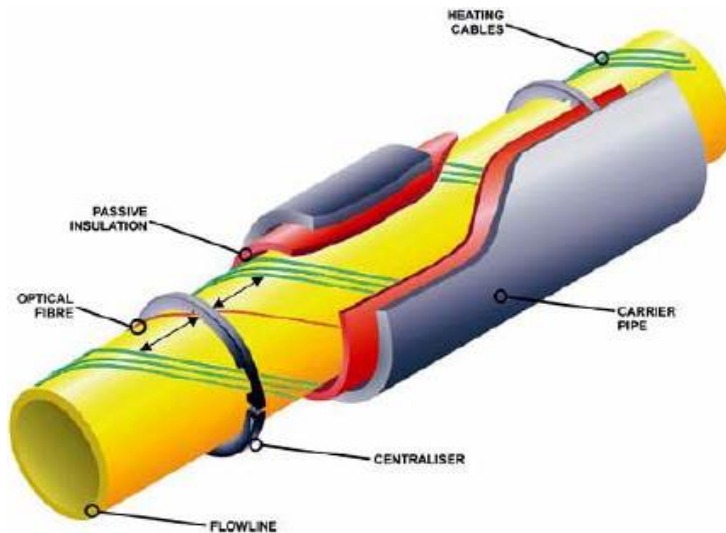


Fig. 20 Electrically heated pipe-in-pipe [44]

9. Thermal Insulation of Subsea Oil and Gas Pipelines

Aerogel is suitable to be used for top insulation efficiency. The flow heat is maintained for the initial few hours, which is longer than for traditional insulation concrete. Paraffin wax + alumina oxide will cool much faster than paraffin wax alone. Using aerogel + paraffin wax + alumina oxide keeps the crude oil warmer for 50 hours. In the last case, the heat just goes back to the crude oil that is inside the pipe [43].

A graphic diagram of the suggested pipe insulation method is seen in Fig. 21. It is comprised of an internal metal pipe (carbon steel), within which hot oil flows, an external pipe, which supplies a barrier against sea water, and insulation materials among these pipes [45]

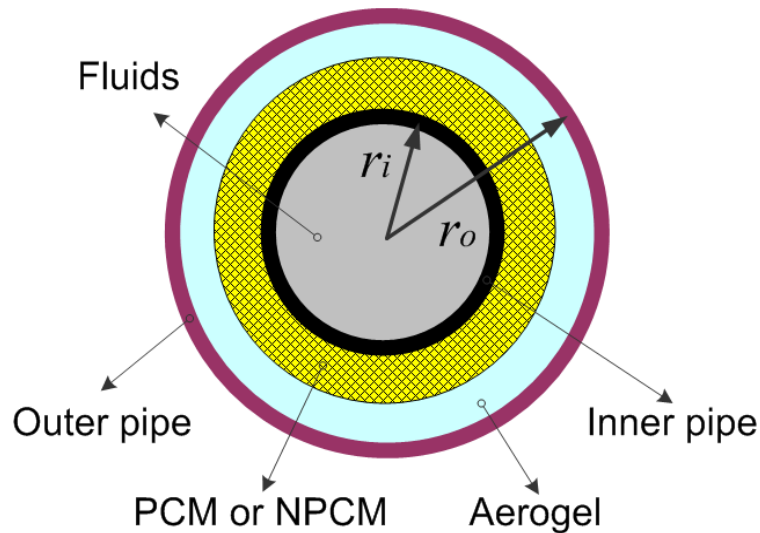


Fig. 21 Schematic of the pipe insulation system [45].

The insulation seen in Fig. 21 is comprised of two coatings: the internal coating is PCM or NPCM, and the external coating is a good traditional insulation material such as aerogel. The impacts of various insulating materials on cool-down time of inner oil are resolved and discussed in this section. Temperature decrease over time is resolved for various insulating materials individually. Fig. 22 and 23 display the impacts of various insulating materials on cool-down time of inner oil. The results include temperature decrease of the warm crude oil without any insulation, with a single coating of different insulation materials, which are aerogel, polyurethane foam, paraffin wax, and NPCM of paraffin wax and alumina oxide.

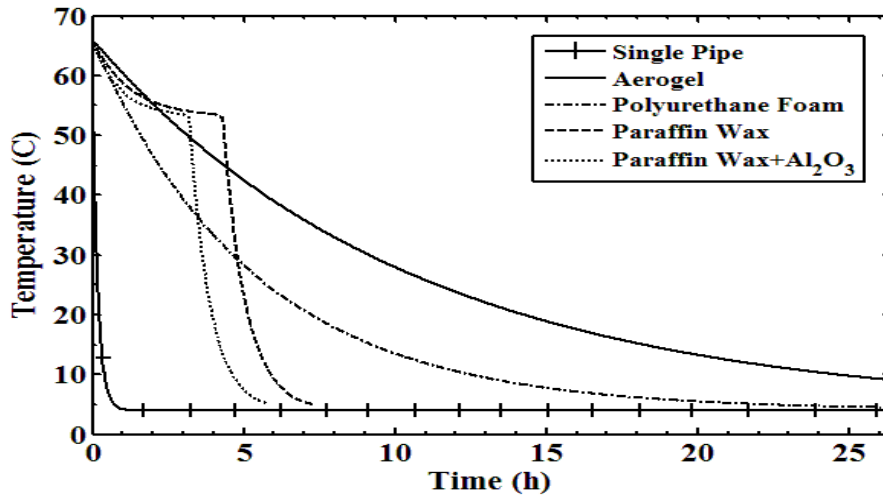


Fig. 22 Cool-down time of internal fluid with a single insulation layer of different materials [45].

It is clear that a simple single pipe without insulation coating raises the thermal balance sea water temperature very quickly. This validates the significance of insulation to decrease cool-down of the oil and postpone hydrate formation in subsea pipelines. In these thermal insulations, aerogel, because of its very low thermal conductivity, achieves good insulation. Utilizing a single PCM or NPCM coating keep the oil warmer, for the first few hours, than utilizing traditional insulation materials.

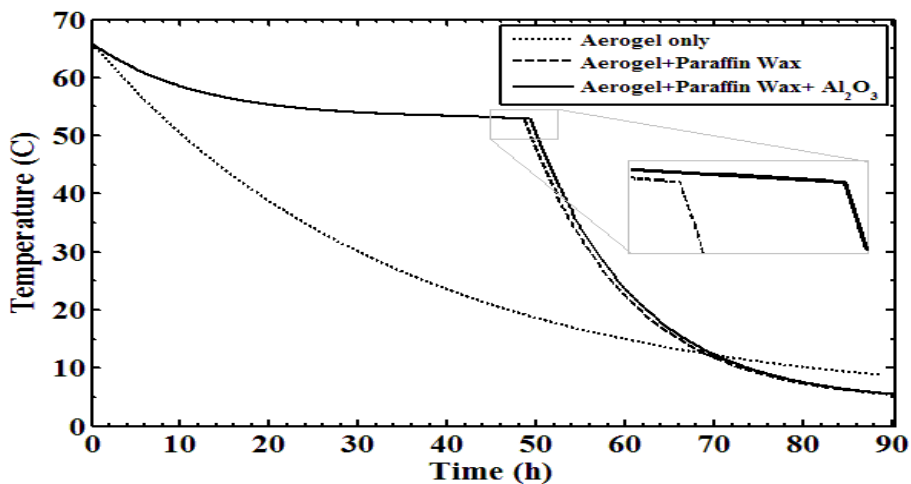


Fig. 23 Cool-down time of internal fluid by combining aerogel insulation with paraffin wax or NPCM [45].

9.1. Friction loss along pipelines

The fluid flow categorizes pipelines into three flow systems, which are laminar flow, transition flow and turbulent flow. Mainly, all these categories are based on the Reynolds numbers which follow [46]:

1. $Re \leq 2000$, laminar flow.
2. $2000 < Re < 3000$, transitional flow.
3. $Re \geq 3000$, turbulent flow.

Reynolds number equation is written [46]:

$$Re = v d / \nu \quad (2)$$

Friction head loss for a pipe is calculated by the Darcy Weisbach equation [46]:

$$h_f = f \frac{l V^2}{d 2g} \quad (3)$$

where Re is Reynolds number, v is average velocity of the fluid (m/s), d is inner diameter for pipeline (m), ν is fluid kinematic viscosity (m^2/s), h_f is friction head loss (m), l is the length of pipeline (m), g is gravitational constant (m/s^2), and f is the friction factor.

9.2. Temperature distribution along pipelines

The aim of obtaining the temperature distribution along pipelines is to make sure the top temperature distribution lowers to a safe zone without hydrate and wax. The equation that follows is used to calculate temperature distribution [46].

$$T_x = T_a + (T_{in} - T_a) \exp\left(\frac{-U\pi D x}{\dot{m} C_p}\right) \quad (4)$$

where T_x is temperature of the crude fluid at location x (m), °C. T_{in} is inlet temperature of crude fluid °C, T_a is ambient temperature of the pipe surroundings °C, d is total pipe outer diameter (m), x is pipeline length from inlet (m), \dot{m} is mass flow rate of crude

fluid kg/s, C_p is specific heat capacity of crude fluid J/kg°C, and U is overall heat transfer coefficient based on pipe of W/m²°C.

9.3. The rate of heat loss

The rate of heat loss from the oil is simply the total rates of heat conduction and convection that are determined from Fourier's law to be [47,48].

$$\dot{Q}_{\text{cylinder}} = -kA \frac{dT}{dr} = U A (T_i - T_o) \quad (5)$$

9.4. Overall heat transfer coefficient

The overall heat transfer coefficient, U , is computed by the following equation [46-49].

$$U = 1 / \sum_i^n R \quad (6)$$

$$\sum_i^n R = R_{\text{film in}} + R_{\text{pipe}} + R_{\text{coating}} + R_{\text{film out}} \quad (7)$$

where

$$R_{\text{film in}} = 1/h_i A_i \quad (8)$$

$$R_{\text{pipe}} = \text{Ln}\left(\frac{r_o}{r_i}\right) / 2\pi r_l k \quad (9)$$

$$\sum R_{\text{coating}} = \text{Ln}\left(\frac{r_{no}}{r_{ni}}\right) / 2\pi r_l k_n \quad (10)$$

$$R_{\text{film out}} = 1/h_o A_o \quad (11)$$

where A is area of heat transfer surface, A_i or A_o (m²), A_i is internal area normal to heat transfer direction, $A_i = 2\pi r_i L$ (m²), A_o is outer area normal to heat transfer direction, $A_o = 2\pi r_o L$ (m²), r_i is internal radius of pipe m, r_o is outer radius of pipe m, r_1 is outer radius of steel pipeline m, r_{no} is outer radius of the coating layer n, r_{ni} is inner radius of the coating layer n, k_{pipe} is thermal conductivity of pipeline W/m°C, k_n is thermal conductivity of coating layer n W/m°C, h_i is internal convection coefficient W/m²°C, h_o is outer convection coefficient W/m²°C.

9.5. Temperature distribution along pipelines.

The aim of this computation is to ensure the fluid temperature through the complete pipeline does not reach the freezing point temperature of the fluid. The equation (5-120) [46,50], is written as following;

$$T_t - T_e = (T_i - T_e)e^{-U\pi DLt/\Sigma mC_p} \quad (12)$$

T_t is temperature of the crude fluid at the time°C. T_e is ambient temperature°C, T_i is initial temperature of the beginning shut down°C, d is outer diameter of insulation pipe (m), m is mass flow rate of crude fluid kg/s, C_p is specific heat capacity for crude fluid pipe insulation layer kJ/kg°C, U is overall heat transfer coefficient W/m²°C, L is the length of pipeline m, and t is the time of the shutdown s.

9.6. Temperature distribution at radius of insulation material

The study assumes a steady state. The following equation calculates temperature for every layer [47,48,51].

$$T_r = \frac{(\ln(r/r_i))}{\ln(r_o/r_i)} (T_o - T_i) + T_i \quad (13)$$

where T_r is temperature distribution of radius, T_o is outer temperature, T_i is inner temperature, r_i is inner radius of pipeline, r_o is outer radius of pipeline, and r is an intermediate radius for which the temperature is sought.

CHAPTER THREE: METHODOLOGY

1. Design

Supplying reliable subsea pipeline systems requires that detailed designs conform to international standards. The initial task is to collect information about the operational design requirements in order to have a notion about working features that leave nothing to be assumed. The design should be based on the chemical composition of the flow to be transported through the pipeline, the high and low pressure at the upstream and downstream ends, and the temperature of the flow for the length of the pipeline. Design factors also include bathymetric and topographic input, particularly the positions and heights of the termination points, obtainable geotechnical information about the subsea properties, oceanographic information about the pipeline's sea environment and every identified constraint on the route specifics (politics, environment, other uses of the ocean) [52]. Many of the recently developed high temperature and high pressure (HT/HP) reservoirs in the North Sea are limited, using pipe bundles and single pipe-in-pipe designs as shares of subsea tie-backs to existing platforms. A reservoir conditions the flowlines to be insulated to avoid wax and hydrate creation as the product cools down along the length of the pipeline. High pressure and high temperature flowlines need thermal insulation to avoid cooling of the well jet flow to prevent wax and hydrate deposition. There are several thermal layers present useful for conventional steel pipe but they tend not to have robust mechanical properties and have not been confirmed at the temperatures now encountered in the HP/HT field, which usually reach 150°C and over. An array of pipelines as a package (pipes-in-pipes) is useful and there are many advantages to grouping separate pipelines together to form a package. The whole package may be transported to its destination and put together at a much lower cost relative to other methods. The increased required

steel needed for the carrier pipe and spacers can be justified by following cost features. A transporter flowline can include more than a single pipeline. “Common applications have also contained control lines hydraulic hoses, power cables, glycol lines etc” [53]. Insulation of the package using gel foam or inert gas is typically less expensive than single pipeline insulation. In many situations, “there is no trenching or burial requirement due to the carrier pipe’s large diameter” [53]. As there are several pipelines in the transporter, subsea congestion in the field is similarly minimized. Usually, pipelines less than 16 inches in diameter are trenched or buried. When contained within a sleeve pipe, which can vary from 18 inches to 24 inches diameter for separate pipe-in-pipe systems and much more for packages, a reasoned argument for non-trenching can be made by demonstrating that the line will not pose a hazard to human life or the environment; nor will it be a danger to other users of the ocean [53].

1.1. Some considerations for insulation

After the design, pipe-in-pipe system thermal analysis is performed including heat transfer. The principal requirements of an insulated pipeline system are:

- To confirm that the product reaches top side with a temperature higher than temperature when wax appears.
- To prevent hydrate formation along the length of the pipeline.
- In the case of a shutdown, to reduce the rate of cool-down to allow enough time for the flow to reject wax and the hydrate to prevent the wax or hydrate formation temperature at any location in the pipeline [53].

1.2. Insulation and heating process

The following requirements associated with insulation and heating of the pipeline system must include:

- Through the normal process, the temperature will be over the hydrate creation temperature for the process.
- Low temperature for the production flowlines will be above the hydrate creation temperature.
- Minimum of certain hours' shutdown will be known before the fluid in the production flowlines has reached the hydrate formation temperature.
- Melting wax will allow the transport temperature in the process to reach an operable degree.
- Thermal projects involve both steady state and transient heat transfer analyses. In the steady state process, the produced crude oil temperature reduces as it flows through the flowline due to the heat transfer through the pipeline wall to the surroundings [53].

2. Physical Model

A schematic diagram illustrates a sample of an insulated pipeline, and includes hot crude oil flow and insulation materials with several thicknesses. The model consists of a single metal carbon steel pipe covered by coating insulation, which is exposed to the seawater. The insulated pipeline considered in this research is presented in Fig. 24 and includes a segment of a straight insulated pipeline and a cross section with several thicknesses. The insulated pipeline is installed at the pressure and temperature of the seawater. This pipeline is used during startup of the crude oil. Shutdowns consider both the fully buried insulated pipeline and the exposed insulated pipeline in sea water. Both cases are considered and validated in the study.



Fig. 24 The segment of a straight insulated pipeline.

2.1 Geometrical parameters of pipeline

The geometrical parameters of pipeline and insulation materials are as follows:

Table 1 Geometrical parameters of pipeline and insulation [45,54].

Internal diameter of pipeline (m)	External diameter of pipeline (m)	Thickness of pipeline (m)	Thicknesses of insulation (m or in)	Length of pipeline (m)
0.273	0.297.7	0.0247	0.0254 (1in)	8,047
-	-	-	0.0381(1.5in)	-
-	-	-	0.0508(2in)	-
-	-	-	0.0635(2.5in)	-

Thermal properties of crude oil, steel pipe, soil and insulation materials used in analysis model are listed in table 2 as follows:

Table 2 Thermal properties of materials [13,20,24,45,54].

Materials	Thermal conductivity W/m K	Density kg/m ³	Specific heat k _j /kg. K	Dynamic viscosity Kg/m s	Flow rate m ³ /day
Steel pipe	60.5	7854	432	–	–
Crude oil	0.13	877	1023	0.0279	8,250
Polyurethane foam	0.04	45	1400	–	–
Aerogel	0.02	140	950	–	–
Polyurethane Aerogel	0.017	180	–	–	–
Soil	0.85	–	–	–	–
Polyethylene	0.35	–	–	–	–
Polypropylene	0.22	–	–	–	–
Polyurethane	0.12	–	–	–	–

2.2 Mathematical model for steady and transient flowline temperature

The model has the following assumptions. Friction induced heat is unimportant, heat transfer in the radial direction is completely controlled by the insulation and the specific heat of the fluid is constant [55].

2.3 Governing equations

Assume the heat flow through a time of Δt . The heat balance equation is written as follows [54,55]:

$$q_{in} - q_{out} - q_R = q_{acc} \quad (14)$$

The terms are defined as follows. q_{in} is the heat energy transported into the pipe by fluid due to convection, q_{out} is the heat energy transported away from the pipe by fluid due to convection, q_R is the heat energy transferred through the insulation layer due to conduction, q_{acc} is the heat energy accumulation in the fluid. These terms can be written as follows [54,55]:

$$q_{in} = \rho C_p v A T_L \Delta t \quad (15)$$

$$q_{out} = \rho C_p v A T_{L+\Delta L} \Delta t \quad (16)$$

$$q_R = 2\pi R k \Delta L \frac{\partial T}{\partial r} \Delta t \quad (17)$$

$$q_{acc} = \rho C_p A \Delta L \Delta T \quad (18)$$

where C_p is the specific heat at constant pressure, J/kg. °C. ρ is the fluid density, kg/m³. v is the average flow velocity of fluid in the pipe, m/s. A is the cross-sectional area of pipe open for fluid flow, m². T_L is the temperature of the fluid in the pipeline; °C. S is the thickness of the insulation layer. R_n is the internal radius of the insulation layer, m. k_n is the thermal conductivity of the insulation layer, W/m °C. ΔL is the length of the pipe segment, m and $\partial T/\partial r$ is the radial temperature gradient in the insulation layer, °C/m.

Substituting equations (15) through (18) into equation (14) results in [54, 55]:

$$\rho C_p v A T_L \Delta t - \rho C_p v A T_{L+\Delta L} \Delta t - 2\pi R k \Delta L \frac{\partial T}{\partial r} \Delta t = \rho C_p A \Delta L \Delta T \quad (19)$$

$$\rho C_p v A \Delta t (T_L - T_{L+\Delta L}) - 2\pi R k \Delta L \frac{\partial T}{\partial r} \Delta t = \rho C_p A \Delta L \Delta T \quad (20)$$

Splitting all the terms of this equation via $\Delta L \Delta t$ results in:

$$\rho C_p v A (T_L - T_{L+\Delta L}) - 2\pi R k \Delta L \frac{\partial T}{\partial r} = \rho C_p A \Delta L \frac{\Delta T}{\Delta t} \quad (21)$$

For extremely small values of ΔL and Δt this equation becomes as follows [54, 55]:

$$v \frac{\partial T}{\partial L} + \frac{\partial T}{\partial t} = - \frac{2\pi R k}{\rho c_p A} \frac{\partial T}{\partial r} \quad (22)$$

The radial temperature gradient in the insulation layer can be written as [54, 55]

$$\frac{\partial T}{\partial r} = T - T_o - G \cos(\theta) L / S \quad (23)$$

where, T_o is the temperature of the medium outside the insulation layer at L equals zero, °C. G is the geothermal gradient, °C/m. θ is the inclination time degree. S is the thickness of the insulation layer, m.

The substitution of equations (23) into (22) results in [54,55]:

$$v \frac{\partial T}{\partial L} + \frac{\Delta T}{\Delta t} = aT = bL + c \quad (24)$$

where parameters are written as [54, 55]

$$a = \frac{2\pi Rk}{\rho C_p s A} \quad (25)$$

$$b = aG\cos(\theta) \quad (26)$$

$$c = -aT_o \quad (27)$$

2.4 Heat transfer and temperature for steady-state fluid flow

The equation for internal temperature profile in steady flow is written as follows

[54, 55]:

$$T = \frac{1}{\alpha^2} [\beta - \alpha\beta L - \alpha\gamma - e^{-\alpha(L+c)}] \quad (28)$$

where the constants are written as:

$$\alpha = \frac{2\pi Rk}{v\rho C_p s A} \quad (29)$$

$$\beta = \alpha G\cos(\theta) \quad (30)$$

$$\gamma = -\alpha T_o \quad (31)$$

$$c = -\frac{1}{\alpha} \ln(\beta - \alpha^2 T_s - \alpha\gamma) \quad (32)$$

where T is the temperature inside the pipe, L is the longitudinal distance from the fluid entry point, R is the internal radius of the insulation layer, k is the thermal conductivity of the insulation material, v is the average flow velocity of fluid in the pipe, ρ is the fluid density, C_v is the heat capacity of fluid at constant pressure and s is the thickness of insulation layer. A is the internal cross sectional area of pipe, G is the principal thermal gradient outside the insulation, θ is the angle between the principal thermal gradient and the pipe orientation, T_o is the temperature of the outer medium at the fluid entry location and T_s is the temperature of the fluid at the fluid entry point.

The rate of heat transfer across the insulation layer over the whole length of the pipeline is written as [54, 55]:

$$q = \frac{2\pi Rk}{s} \left(T_o L - \frac{G\cos(\theta)}{2L^2} - \frac{1}{\alpha^2} \left\{ (\beta - \alpha\gamma)L - \frac{\alpha\beta}{2L^2} + \frac{1}{\alpha} [e^{-\alpha(L+c)} - e^{-\alpha c}] \right\} \right) \quad (33)$$

where q is the rate of heat transfer (heat loss).

2.5 Transient temperature during startup

The internal temperature profile after starting up an oil flow is written as follows [54, 55]

$$T = \frac{1}{\alpha^2} \{ \beta - \alpha\beta L - \alpha\gamma - e^{-\alpha[L+f(L-vt)]} \} \quad (34)$$

where function f is written:

$$f(L - vt) = -(L - vt) - \frac{1}{\alpha} \ln \{ \beta - \alpha\beta(L - vt) - \alpha\gamma - \alpha^2 [T_s - G\cos(\theta)(L - vt)] \} \quad (35)$$

2.6 Transient temperature through flow rate change

Assume that when the flow rate is increased or decreased in a pipeline, the crude oil changes to a new velocity, v' , in the pipe. The internal temperature profile is written as follows [54, 55]:

$$T = \frac{1}{\alpha'^2} \{ \beta' - \alpha'\beta'L - \alpha'\gamma' - e^{-\alpha[L+f(L-v't)]} \} \quad (36)$$

where constants are:

$$\alpha' = \frac{2\pi Rk}{v'\rho C_p} \quad (37)$$

$$\beta' = \alpha' G\cos(\theta) \quad (38)$$

$$\gamma' = -\alpha'T_o \quad (39)$$

where function f is written as [54, 55]:

$$f(L - v't) = -(L - v't) - \frac{1}{\alpha'} \ln \{ \beta' - \alpha'\beta'(L - v't) - \alpha'\gamma' - \left(\frac{\alpha'}{\alpha}\right)^2 \{ (\beta' - \alpha'\beta'(L - v't) - \alpha'\beta' - e^{-\alpha[L+f(L-v't+c)]} \} \} \} \quad (40)$$

where t is the time. Assume that when the flow rate is increasing or decreasing in the pipeline, the fluid changes to a new velocity, v' , in the pipeline.

2.7 Convection

Both the internal and external surfaces of a subsea pipeline have boundary layers with fluids and the pipeline surface and the fluids have different temperatures, which cause

convection heat transfer. In flow assurance evaluation, the heat transfer coefficient is similarly termed as the film heat transfer, as convection occurs at a film layer of fluid at the pipeline surface [20,56].

2.8 Internal heat transfer coefficient

Liquid properties in the same flow velocity and the pipeline diameter have an effect on the internal heat transfer coefficient, which occurs between the pipeline's internal surface and the flowline in the pipeline. For the internal heat transfer coefficient of pipelines the subsequent dimensionless correlation is for the fully turbulent flow of single phase fluids. The Reynolds number for laminar flow is $Re_i < 2100$ and the Nusselt number may be calculated by the following equation [20,46,56].

$$N_{ui} = 3.66 + \frac{0.0688 \left(\frac{d_i}{L_i}\right) Re_i Pr_i}{1 + 0.4 \left[\left(\frac{d_i}{L_i}\right) Re_i Pr_i\right]^{2/3}} \quad (41)$$

where, the L_o , the length of the pipeline from inlet and point is measured. Almost all pipelines cases are, $d_i/L_o \approx 0$. For this reason, Eq. (41) becomes [20,46,56]:

$$N_{ui} = 3.66 \quad (42)$$

When the fluid is in the case transition region ($2100 < Re_i < 10^4$), the heat transfer in this region is always uncertain, because of the unsteady nature of the flow and especially for the multiphase flow in pipeline systems. A correlation projected may be used to estimate h_i in this area [20,46, 56]:

$$N_{ui} = \left(\frac{f}{8}\right) (Re_i - 1000) Pr_i + 12.7 \left(\frac{f}{8}\right)^{2/3} (Pr_i^{2/3} - 1) \quad (43)$$

In all cases the friction factor f may be obtained as shown in the Moody diagram for smooth pipes [20,46,56]:

$$f = [0.79 \ln(Re_i) - 1.64]^{-2} \quad (44)$$

This correlation is effective for $0.5 < Pr_i < 2000$ & $3000 < Re_i < 5 \cdot 10^6$ [20,46,56].

The following equation used for the fully turbulent flow, from [20,46,56] can

be used to estimate heat transfer coefficient, h_i :

$$Nu = 0.0255 Re_i^{0.8} Pr_i^n \quad (45)$$

where Nu_i is the Nusselt number, $Nu_i = h_i d_i / k_f$,

Re_i is the Reynolds number, $Re_i = d_i V_f \rho_f / \mu_f$ and

Pr_i is the Prandtl number, $Pr_i = C_{p,f} \mu_f / k_f$, $n = 0.4$ if the fluid is heated and $n = 0.3$ if

the fluid is cooled, h_i is internal convection coefficient, $W/m^2 K$, d_i is the pipeline

inside diameter, m, k_f is the thermal conductivity of the flowing liquid, $W/m K$, V_f is

the velocity of the fluid, m/s, ρ_f is the density of the fluid, kg/m^3 , μ_f is the viscosity of

the fluid, pa.s and $C_{p,f}$ is the specific heat capacity of the fluid, $J/kg K$.

2.9 External heat transfer coefficient

The correlation of average external heat transfer coefficient is calculated by the equation following, from [20,46,56]:

$$Nu_o = c Re_o^m Pr_o^{\frac{1}{3}}$$

(46)

where, Nu_o , Nusselt number, $Nu_o = \frac{h_o d_o}{k_o}$,

Re_o Reynolds number, $Re_o = \frac{d_o V_o \rho_o}{\mu_o}$,

Pr_o Prandtl number, $Pr_o = \frac{C_{p,o} \mu_o}{k_o}$,

where, h_o is the external convection coefficient, $W/m^2 K$, d_o is the pipeline outer

diameter, m, k_o is the thermal conductivity of the surrounding fluid, $W/m K$, V_o is the

velocity of the surrounding fluid, m/s, ρ_o is the density of the surrounding fluid, kg/m^3 ,

μ_o is the viscosity of the surrounding fluid, pa.s, $C_{p,o}$ is the specific heat capacity of the

surrounding fluid, $J/kg K$ and C, m are constants, dependent on the Re number range.

2.10 Heat transfer coefficient for fully buried pipeline

The heat transfer is not constant for a buried pipeline. Therefore, a simulated thickness of the soil is used to account for the asymmetries of the system. Using a conduction profile factor for a horizontal pipe buried in a semi-infinite medium, the heat transfer coefficient for a buried pipeline is written as follows [20,46,56]:

$$h_{\text{soil}} = k_{\text{soil}} / \left(\frac{d}{2}\right) \cosh^{-1}\left(\frac{2z}{d}\right) \quad (47)$$

where h_{soil} is the heat transfer coefficient of the soil, $\text{W/m}^2 \text{K}$, k_{soil} is the thermal conductivity of the soil, W/m K , d is the outside diameter of the buried pipe, m , z is the distance between the top of the soil and the center of the pipeline, m .

For the example of $z > d/2$, $\cosh^{-1}(x)$ can be simplified so that $\ln[x + (x^2 - 1)^{0.5}]$ gives [20,46,56]:

$$h_{\text{soil}} = 2k_{\text{soil}} / d \ln[2z + \sqrt{4z^2 - d^2}] / d \quad (48)$$

2.11 Overall heat transfer coefficient for unburied and buried pipelines

The U-value is calculated by equation (2-5), as written in chapter two. Using insulated flowlines, the thermal insulation materials' layers or burial require an order of magnitude of more thermal resistance than both the internal and external heat transfer coefficients. Consequently, the special effects of the internal and external heat transfer coefficient on the overall heat transfer coefficient of the flowlines may be unseen and the overall heat transfer coefficient of the flowlines can be written as follows [20]:

$$U = 1 / \left[\sum r \ln\left(\frac{r_{\text{no}}}{r_{\text{in}}}\right) / k_n + r_i \cosh^{-1}\left(\frac{2z}{d_o}\right) / k_{\text{soil}} \right] \quad (49)$$

In the all cases the denominator presented above has two terms: the first term is the thermal resistance of the radial layers of steel and insulation coatings and the second term is the thermal resistivity due to the soil and is valid for $H > d/2$. If the internal and

external heat transfer coefficients are to be combined, the external heat transfer coefficient usually only comprises unburied flowlines. For simple buried flowlines, where the soil offers fundamentally all of the flowline's thermal insulation, there is a near linear relationship between the overall heat transfer coefficient and the thermal conductivity of soil, k_{soil} . For buried and insulated flowlines, the impact of thermal conductivity of soil, k_{soil} , on the overall heat transfer coefficient is less than for simple buried flowlines [20].

3. Geometric Modeling of ANSYS Fluent Computation Fluid Dynamic (CFD)

Given the geometry related to the mathematical modeling of the procedures presented in Table 1 above, only the length is considered in a sample of three meters for mathematical modeling. If the tube surface condition is fixed by imposing either a uniform temperature (T_s is constant) or a uniform heat flux (q_s is constant), a thermally fully developed condition is eventually reached. The shape of the fully developed temperature profile $T(r,x)$ differs depending on whether a uniform surface temperature or heat flux is maintained [48]. It is generally agreed that the entrance effects are confined within a tube length of 10 diameters [47]. Turbulent, fully developed, $0.5 \leq P_r \leq 2000$, $3000 \leq R_e \leq 5 * 10^6$, $(L/D) \geq 10$ [48]. This research has been done using the Reynolds number (Re) = 25,000 and Prandtl number (Pr) = 200. Furthermore, they are in agreement with the results in reference [48]. The maximum allowable number of nodes is $0.5 * 10^6$. Because of the software's licensed instruction, a smaller length had to be chosen. However, the finding from this small scale-study is valid for the large length. We were ensure that the flow was fully developed in the small-scale study. Essentially these two systems are similar hydrodynamically. The pipeline is produced with three coatings respectively, which are the fluid domain, steel

pipe layer and insulation material layer. Fig. 25 presents a sketch of the simulation modeling. The analysis model is presented in ANSYS 17.2 Workbench.

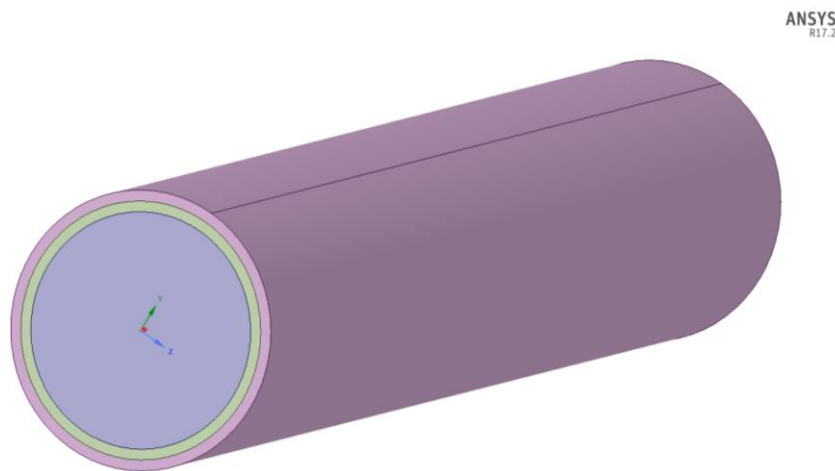


Fig. 25 Sketch of simulation modeling.

4. Mesh Simulation Modeling

A mesh is generated with three interfaces to provide a high speed of modeling, which are the fluid domain, steel pipe layer, and insulation layer. Firstly, a default mesh needs to be developed using size and inflation. The size function controls the growth and circulation of the mesh in important areas of high curvature or closeness of surfaces. This size is used to develop meshing for all edges, faces and bodies for which a span angle center is chosen: for fine mesh, the min size is 0.001, max face size is 0.02, and max element size is 0.02. Inflation is used to generate prism faces of the body and edges, which are used consecutively, as mentioned in the geometry. Details of the inflation consist of the following: the boundary is two faces, inflation option is smooth transition, transition ratio is default 0.272, maximum layers are 10 and the growth rate is 1.2. The mesh is generated with the details mentioned and has 199876 nodes and 468530 elements with a successful translation to Fluent and obtains good results for all requirements. Fig. 26 presents the mesh of the pipeline.

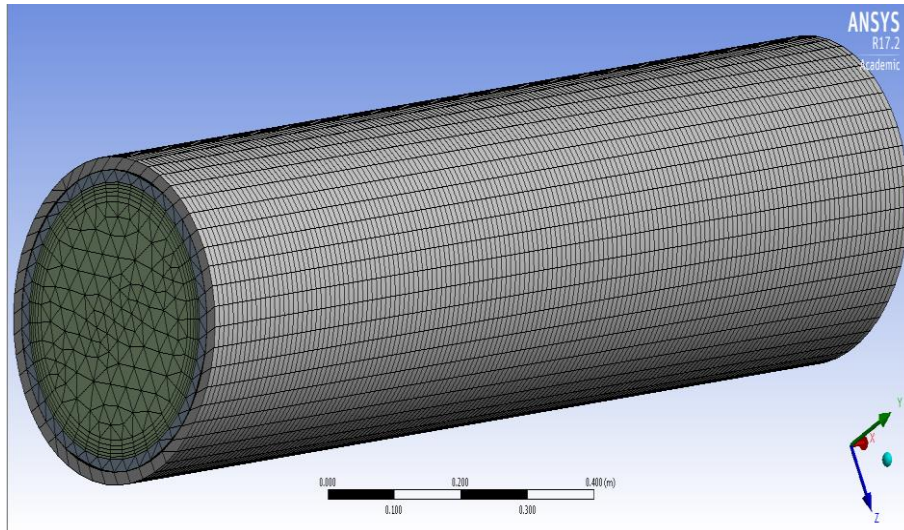


Fig. 26 Mesh of pipeline

5. Setup

From the Fluent CFD home screen, transient calculation was selected from the setup menu. Models were then selected which turned the energy on. Thermal properties were entered by selecting the materials tab and inputting the Fluent database from the dropdown menu. The boundary conditions tab was then selected and the inlet, outlet, and wall of the pipeline is modeled. Then from the solution initialization, tab hybrid initialization was selected after which the calculation activities tab was opened, where the solution data export was chosen. Finally, run calculation was selected where time step size was inputted as 0.0015 sec, the number of time steps as 10,000, and max iterations as 20 steps.

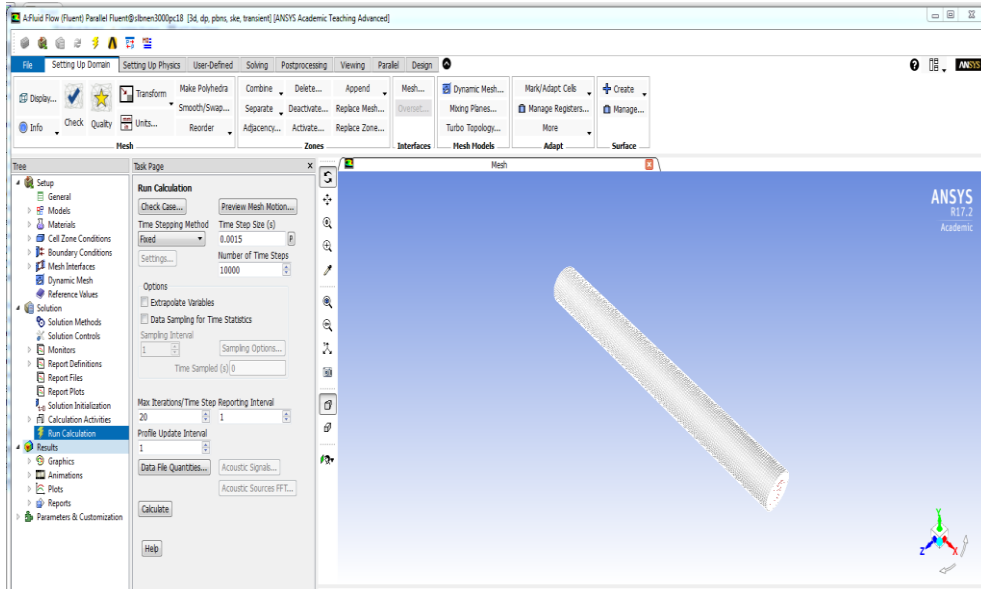


Fig. 27 Run calculation of setup.

6. Heat Transfer Modeling in Fluent CFD

6.1 Energy transport equation

ANSYS Fluent solves the energy equation and is written in the following form [57]:

$$\partial(\rho E)/\partial t + \nabla [v(\rho E + \rho)] = \nabla \left(k_{\text{eff}} \nabla T - \sum_j h_{jJ_j} + (\tau_{\text{eff}} v) \right) + s_h \quad (50)$$

where k_{eff} is the effective conductivity $k+k_t$, k_t is the turbulent thermal conductivity, defined according to the turbulence model being used, and J_j is the diffusion flux of species j . The first three terms on the right-hand side represent energy transfer due to conduction, species diffusion and viscous dissipation, respectively.

s_h includes volumetric heat sources that have been defined.

Energy equation per unit mass is defined as follows [57]:

$$E = h - \frac{p}{\rho} + \frac{v^2}{2} \quad (51)$$

where sensible enthalpy h is defined for incompressible fluids, written as [58]:

$$h = \sum_j Y_j h_j + \frac{p}{\rho} \quad (52)$$

in equation (3-39) Y_j is the mass fraction of species j , written as [58]:

$$h_j = \int_{T_{ref}}^T C_{p,j} dT \quad (53)$$

The value used for T_{ref} in the sensible enthalpy estimation depends on the solver and simulations in the system. The pressure based solver T_{ref} is 298.15k except for models for which case T_{ref} is an operator input for the species. For the density based solver T_{ref} is acceptable when developing species transport [58].

6.2 Governing Equation

Convection heat transfer is computed by the following equation [57, 58]:

$$q = h(T_{body} - T_{\infty}) = h\Delta T \quad (54)$$

where h is the average heat transfer coefficient W/m^2K in equation (3-41) [58].

Conduction heat transfer is governed by Fourier's law. Fourier's law states that the heat transfer rate is directly proportional to the gradient of temperature [58].

$$q_{conduction} = -k\nabla T \quad (55)$$

The constant of proportionality is the thermal conductivity k . k may be a function of temperature, space, etc. k is a constant value for isotropic materials and k is a matrix.

CHAPTER FOUR: RESULTS AND DISCUSSION

1. Validation between Matlab Program and Digitized Graphs.

The purpose of validation is to investigate the output of the Matlab program. The program contains the same geometric properties as the thermal insulation materials and pipelines [54].

Fig. 28 shows a validation of the transient flow temperature profiles along the length of the steel pipeline between the published digitized graph and the mathematical model for polyethylene insulation. In the first step, a polyethylene layer of 2.54 cm is initially investigated as the insulation. Fig. 28 above shows a validation for the temperature profiles analyzed using Eqs. (28) and (34). From the results presented, which are approximately identical, the error percentage is decreased less than 1%. This shows that at approximately 30 minutes after start-up, the transient temperature profile in the pipeline will approach the steady state flow temperature profile. The temperature at the end of the pipeline will be slightly lower than 20°C under common working conditions. Obviously, this insulation will not meet the design standard of 25 °C for the pipeline as needed.

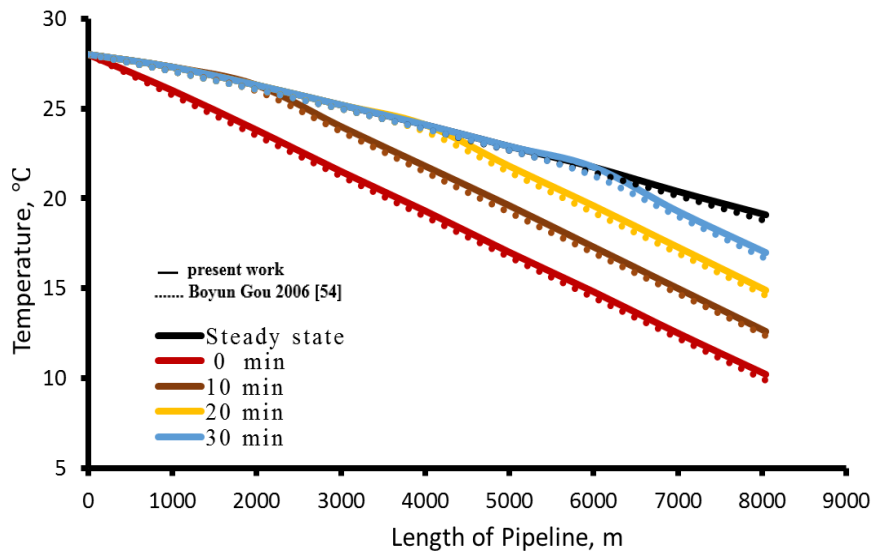


Fig. 28 Validation of transient flow temperature profile on the length of the steel pipeline between digitized graph and mathematical model for polyethylene insulation.

Fig. 29 shows the validation of steady state flow temperature profiles for the length of the pipeline between the published digitized graph and mathematical model for polyethylene insulation. In the first step, Fig. 29 shows the steady state flow temperature sketches analyzed using Eq. (28) with polyethylene layers of four thicknesses. The results presented are approximately identical and decreased approximately 2.3%. This shows that a uniform polyethylene layer 6.35 cm thick does not reach at a pipeline temperature higher than 25°C; consequently, polyethylene should not be considered in this study.

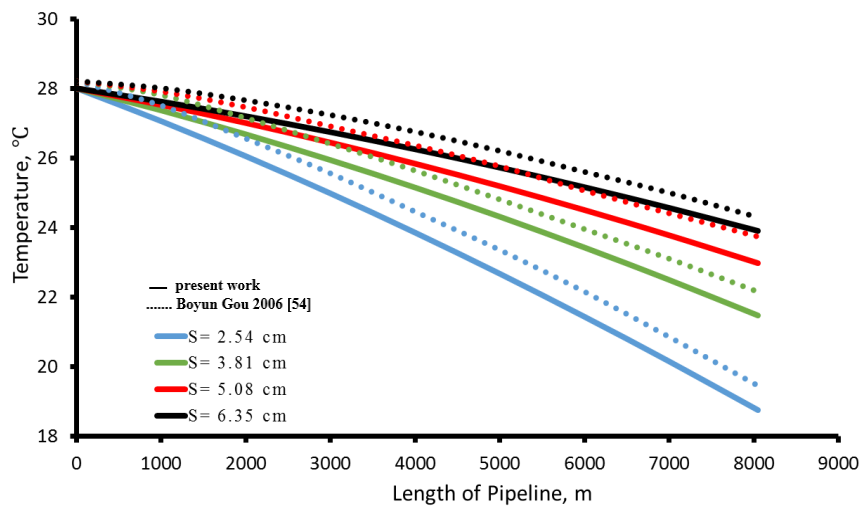


Fig. 29 Validation of steady state flow temperature profile on the length of the steel pipeline between digitized graph and mathematical model for polyethylene.

Fig. 30 shows the validation of transient flow temperature profiles on the length of the steel pipeline between the published digitized graph and the mathematical model for polypropylene insulation. In the first step, a polypropylene layer of 2.54 cm (1 in.) is initially investigated as the insulation. Fig. 30 below shows a validation for the temperature profiles analyzed using Eqs. (28) and (34). The results presented, which are approximately identical, show the error percentage is decreased approximately less than 1%. This indicates that at approximately 30 minutes after startup, the transient temperature profile in the pipeline will approach the steady state flow temperature profile. The temperature at the end of the pipeline will be slightly lower than 20°C under common working conditions. Obviously, this insulation option does not achieve the design standard of 25°C in the pipeline as needed.

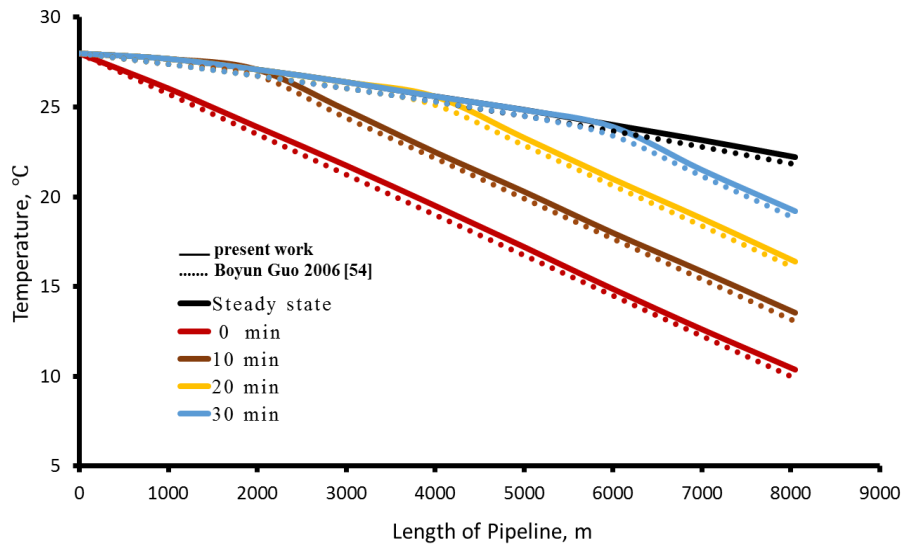


Fig. 30 Validation of transient flow temperature profile on the length of the steel pipeline between digitized graph and mathematical model for polypropylene insulation.

Fig. 31 shows the validation of the steady state flow temperature profiles of the length of the steel pipeline between published digitized graph and the mathematical model for polypropylene insulation. In the first step, Fig. 31 presents the steady state flow temperature profiles analyzed using Eq. (28) with polypropylene layers of four thicknesses. The results are presented and are approximately identical and the error percentage is decreased approximately 2.3%. This shows that even a polypropylene layer 6.35 cm (2.5 in) thick will still not yield a pipeline temperature higher than 25°C; thus, polypropylene is not recommended by this study.

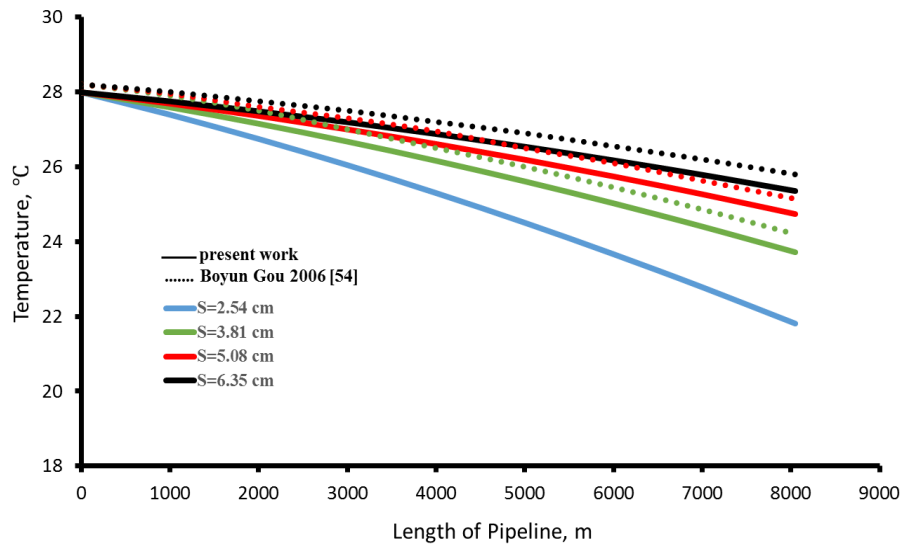


Fig. 31 Validation of steady state flow temperature profile on the length of the steel pipeline between digitized graph and mathematical model for polypropylene insulation.

Fig. 32 demonstrates validation of transient flow temperature profile for the length of the steel pipeline between published digitized graph and the mathematical model for polyurethane insulation. In the first step, a polyurethane layer of 02.54 cm (1in) is initially investigated as the insulation. Fig. 32 above shows a validation for the temperature profiles calculated using Eqs. (28) and (34). The results presented are approximately identical and the error percentage is decreased approximately less than 1%. This indicates that at approximately 30 minutes after start-up, the transient temperature profile in the pipeline will approach the steady state flow temperature profile. The temperature at the end of the pipeline will be slightly lower than 20°C under common working conditions. Obviously, this insulation option does not meet the design standard of 25°C in the pipeline as needed.

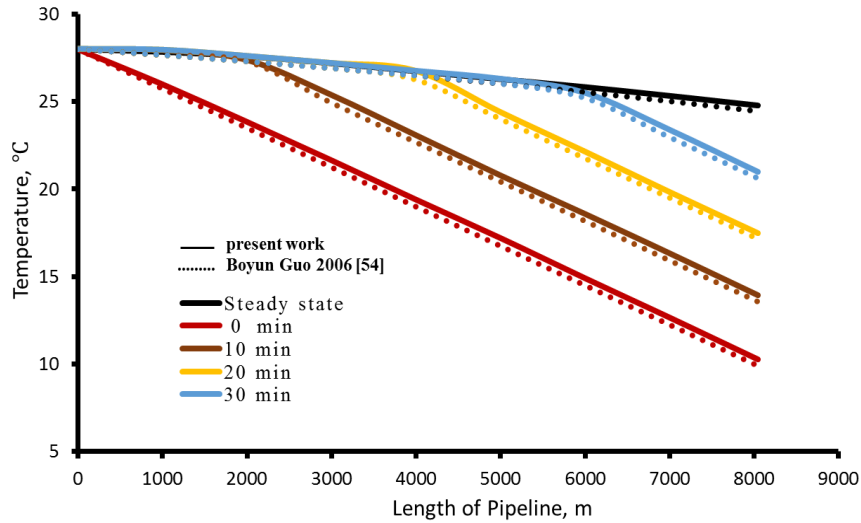


Fig. 32 Validation of transient flow temperature profile on the length of the steel pipeline between digitized graph and mathematical model for polyurethane insulation.

Fig. 33 presents validation of steady state flow temperature profiles for the length of the steel pipeline between the published digitized graph and the mathematical model for polyurethane insulation. In the first step, Fig. 33 shows the steady state flow temperature sketches analyzed using Eq. (28) with polyurethane layers of four thicknesses. The results are presented and are approximately identical; error percentage is decreased approximately 2.3%. This shows that a uniform polyurethane layer 6.35 cm thick will still not provide a pipeline temperature higher than 25 °C; thus, polyurethane is not recommended by the results of this study.

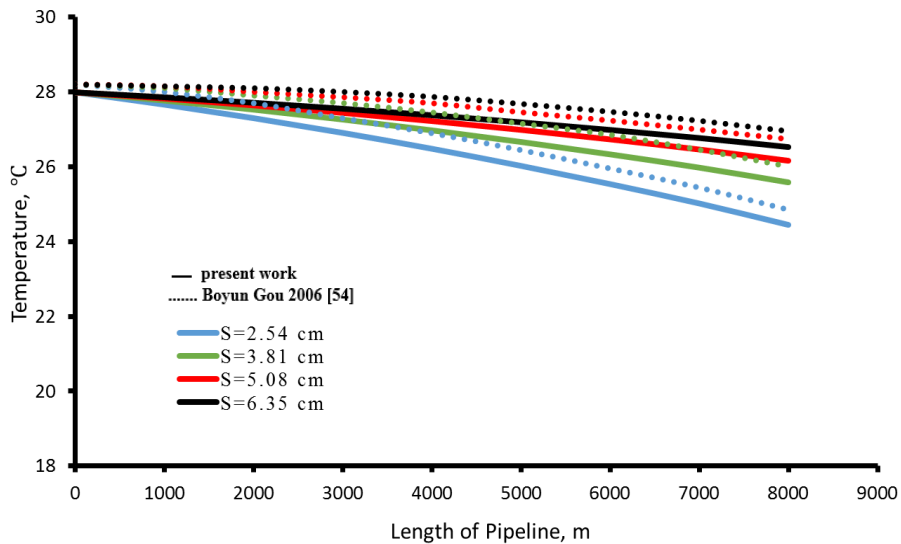


Fig. 33 Validation of steady state flow temperature profile on the length of the steel pipeline between digitized graph and mathematical model for polyurethane insulation.

2. Mathematical Model by Matlab Program

Mathematical model by Matlab program for steady-state flow and transient flow temperature profiles during start-up flowlines. The calculated model presented in chapter three is used to design an underwater pipeline. The main aim of the investigation is to find an appropriate insulation layer thickness and material. The design standard was utilized for this study to confirm that the temperature at the end of the pipeline does not drop lower than 67°C. Insulation materials considered for this design are polyurethane foam, aerogel and polyurethane aerogel.

In this case, a polyurethane foam layer of 2.54 cm is initially investigated as the thickness of insulation is increased to (3.81, 5.08 and 6.35 cm). Fig. 34 below shows a steady state flow temperature sketch analyzed using Eq. (28) with many insulation thicknesses. It demonstrates that a uniform polyurethane foam of 6.35 cm thick will offer a stream line temperature lower than 67°C; thus, polyurethane foam is not recommended for use in this system.

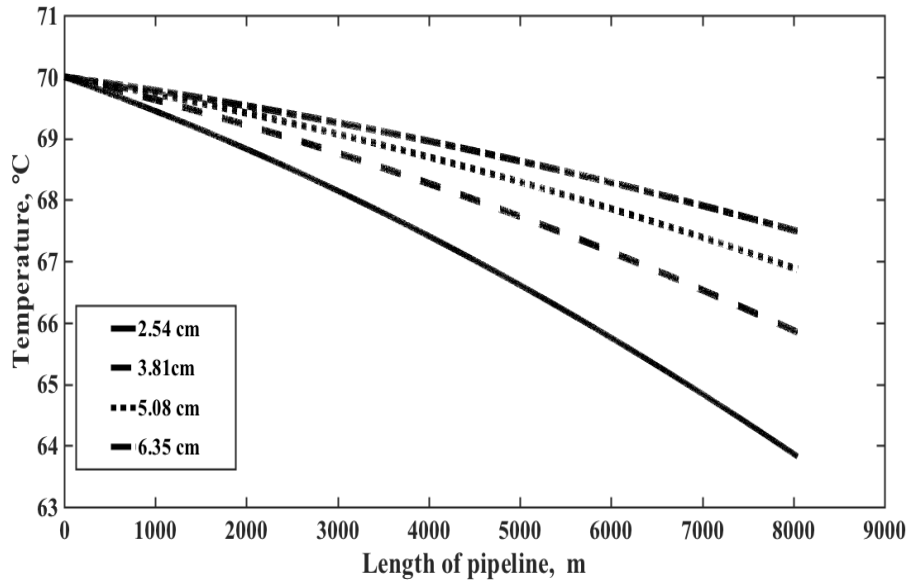


Fig. 34 Steady-state-flow temperature profiles on the length of the steel pipeline with polyurethane foam layers of various thicknesses.

In this case, a polyurethane foam layer of 2.54 cm is initially investigated as the insulation. Fig. 35 above presents the temperature sketches analyzed using Eqs. (28) and (34). These show that at approximately 30 minutes after start-up, the transient temperature, sketched for the pipeline, will approach the steady state flow temperature sketch. The temperature at the end of the pipeline will be slightly lower than 64°C under common working conditions. Obviously, this insulation does not meet the design standard of 67°C in the flowline.

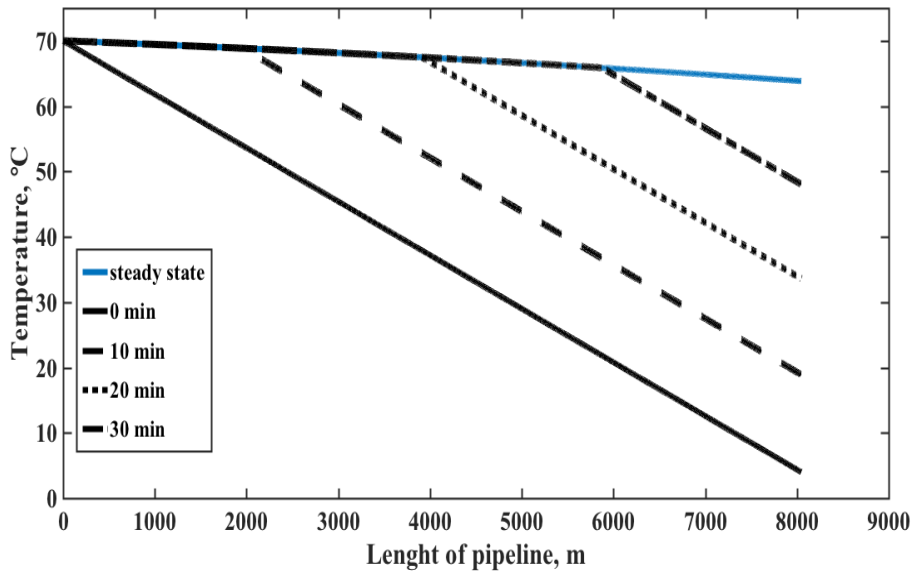


Fig. 35 Transient flow temperature profiles on the length of the pipeline with a polyurethane foam layer of 2.54 cm.

In this case, an aerogel layer of 2.54 cm is first measured and later increased to (3.81, 5.08 and 6.35 cm). Fig. 36 presents the steady state flow temperature sketch analyzed using Eq. (28). This shows that an aerogel layer 3.81cm thick will provide a flow line temperature higher than 67°C; thus, the measured aerogel is close to the design standard at this thick 2.54 cm for this system.

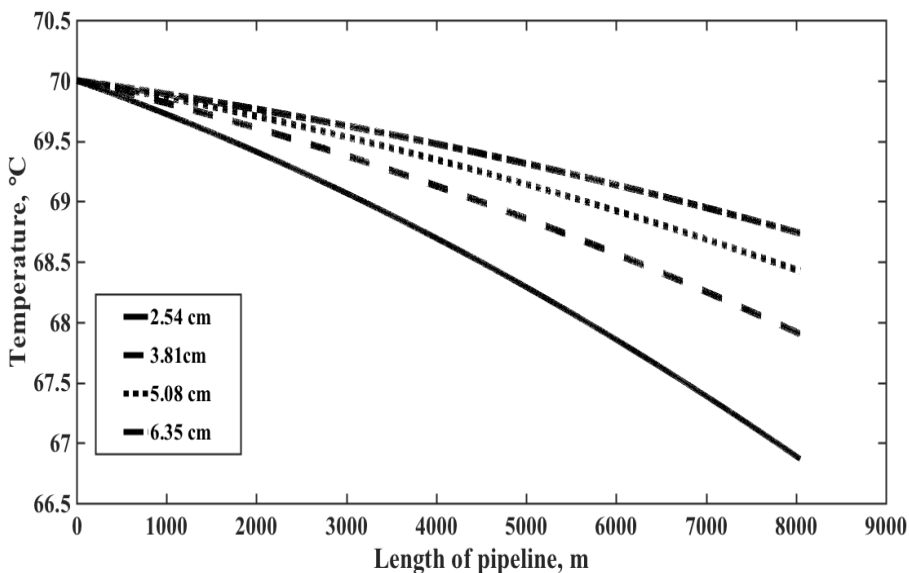


Fig. 36 Steady-state-flow temperature profiles on the length of the steel pipeline with aerogel layers of various thicknesses.

In this case, an aerogel layer of 2.54 cm thick is initially investigated as the insulation. Fig. 37 presents the temperature profiles obtained after analysis using Eqs. (28) and (34). It again appears that at approximately 40 minutes when start-up, the transient temperature in the pipeline will approach the steady state flow temperature profile. The temperature at the end of the pipeline will be approximately 66.8°C under common working conditions. Obviously, this insulation is approximately close to the design standard of 67°C in the flowline.

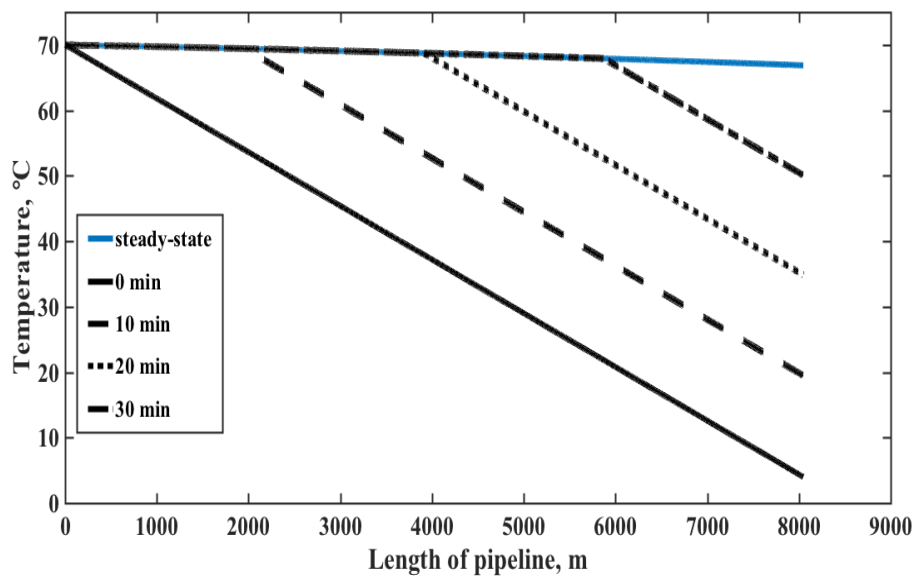


Fig. 37 Transient flow temperature profiles on the length of the pipeline with an aerogel layer of 2.54 cm thick.

In this case, a polyurethane aerogel layer of 2.54 cm is initially investigated and later increased to (3.81, 5.08 and 6.35 cm). Fig. 38 presents the steady state flow temperature profile analyzed using Eq. (28). This shows that a polyurethane aerogel layer of 2.54 cm or more should be chosen for insulation of the flow line which gives a flow line temperature lower than 67°C. The polyurethane aerogel is therefore the best insulation material used for this purpose.

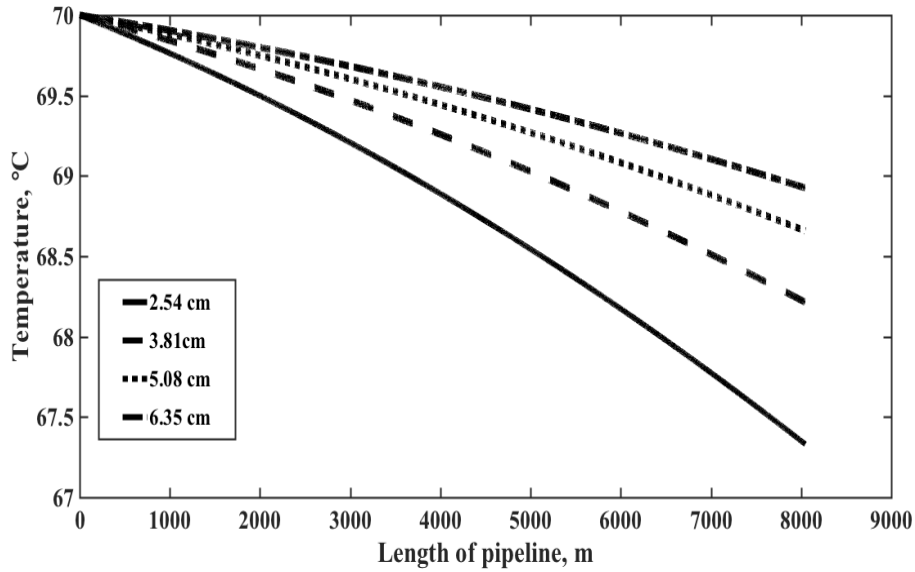


Fig. 38 Steady-state-flow temperature profiles on the length of the steel pipeline with polyurethane aerogel layers of various thicknesses.

In this case, a polyurethane aerogel layer of 2.54 cm is initially investigated as the insulation. Fig. 39 shows the temperature profiles analyzed using Eqs. (28) and (43). It appears that after approximately 40 minutes, the temperature at the end of the pipeline is recorded to be more than 67°C under common working conditions. The polyurethane aerogel for this design keeps the crude oil warm as needed during start-up of the flowline. The polyurethane aerogel has strong mechanical properties against high pressure of more than 7.8 MPa without any breakage, as mentioned in chapter two [24]. The polyurethane aerogel will work in extremely deep ocean water.

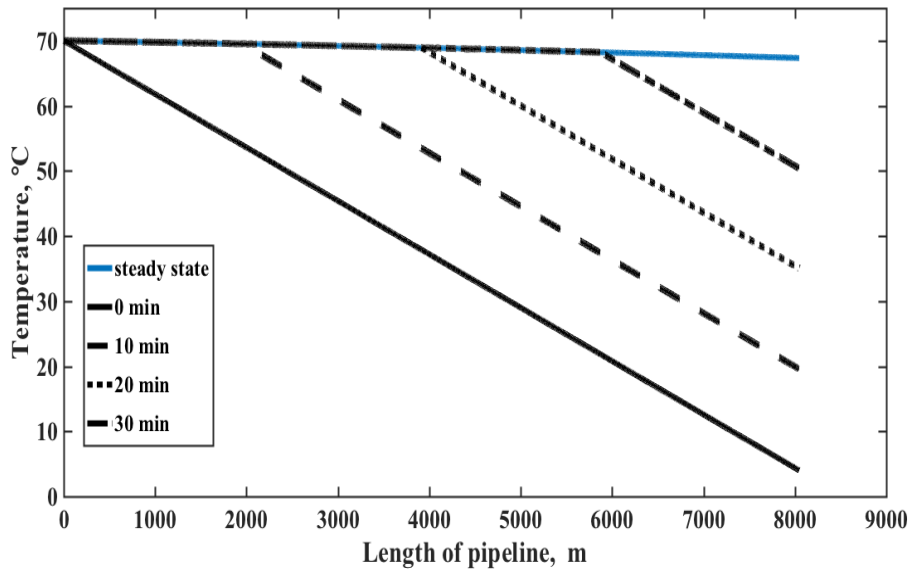


Fig. 39 Transient flow temperature profiles on the length of the steel pipeline with a polyurethane aerogel layer of 2.54 cm.

Table 3 lists the total heat loss for all the steady-state flow cases that were computed by Eq. (33). The calculation was specified along the pipeline. Heat loss values decrease with polyurethane aerogel more than for polyurethane foam and aerogel. Also, increasing the thickness reduces heat loss along the pipelines.

Table 3. Values of heat loss for insulation pipeline with three insulation materials and four thicknesses.

Thicknesses (cm)	Heat loss of insulation materials		
	Polyurethane foam (kw)	aerogel (kw)	Polyurethane aerogel (kw)
2.54	213.68	108	92
3.81	143.5	72	61.5
5.08	108	54	46
6.35	86.6	43.5	37

3. Cool-Down Time during Shutdown Flowline

The effects are for optimal insulation materials with several thicknesses for two cases, an exposed pipeline in seawater and a pipeline buried under seawater, during shutdown. The cool-down time is a significant factor to control the heat loss and temperature drop during shutdown of the pipeline. Thus, the insulation thickness will be created in the lowest cool-down time, using Equation (12).

The impacts of several insulation polyurethane foam thicknesses on cool-down time through shut-down of a flowline are computed in transient temperatures. Temperature over time is calculated for steel pipelines both without insulation and with several thicknesses of insulation material. Fig. 40 presents the results of heat loss over time for the different insulation thicknesses. When the steel pipe does not have an insulation layer it always reaches the thermal equilibrium (environment temperature) in less than one hour. However, using an insulation layer reduces heat loss of pipelines and cool-down time increases as insulation thickness increases. Pipelines with an insulation layer of 6.35 cm reach seawater temperature after 22 hours.

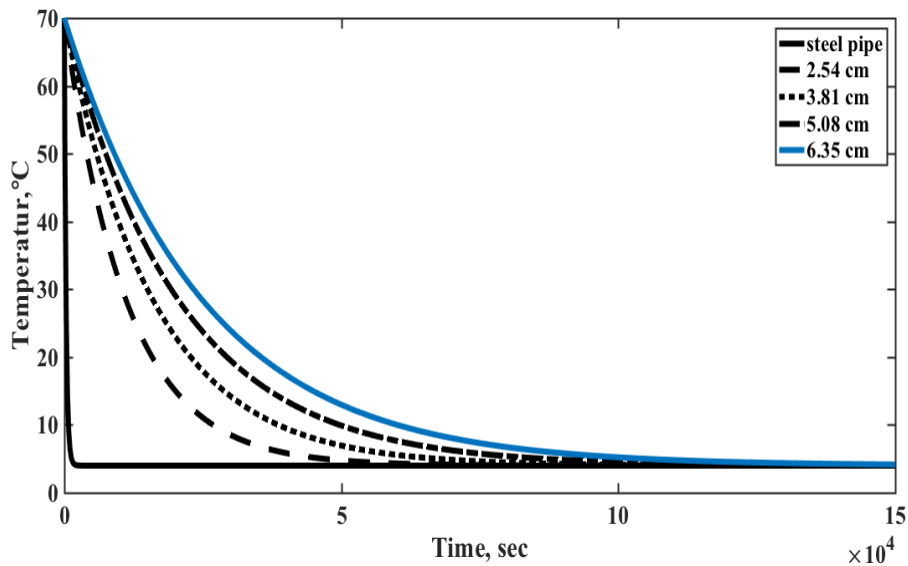


Fig. 40 Cool-down time temperature profiles during shutdown with several insulation thicknesses of polyurethane foam exposed pipeline in seawater.

The impacts of several insulation aerogel thicknesses on cool-down time through the shutdown flowline are computed at transient temperatures. Due to its low thermal conductivity, these results demonstrate that aerogel has the longest cool-down time, meaning that the pipelines keep the crude oil warmer for longer, which will postpone hydrate formation in seabed pipelines. Fig. 41 presents the evaluation results for cool-down time using aerogel as an insulation layer. The temperature decreases over time

for the different insulation thicknesses are displayed in the results. An insulation layer of 2.54 cm reduces pipeline's heat loss and thermal equilibrium occurs after 15 hours. As insulation layers are added increased cool-down time is achieved. Thermal equilibrium occurs after 42 hours for an insulation layer of 6.35 cm. At this time point the temperature is 8°C.

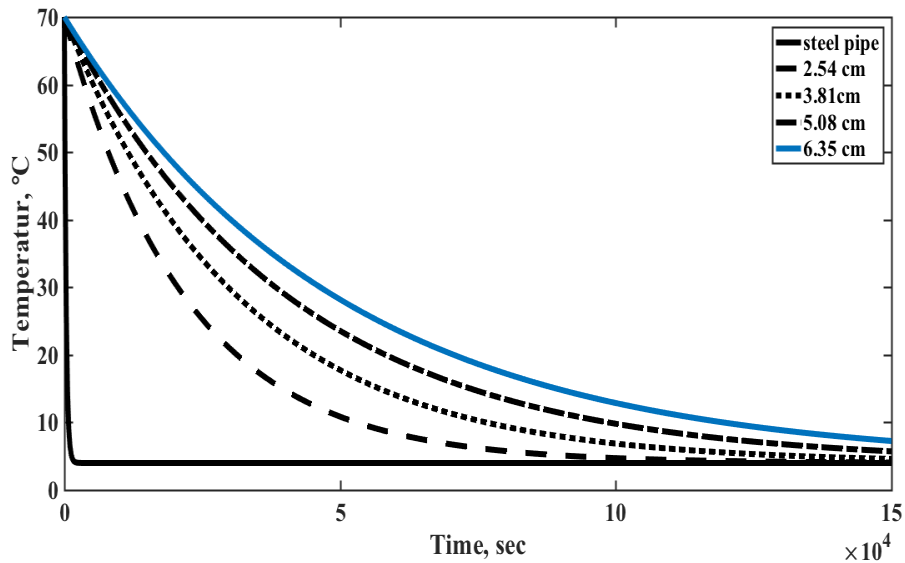


Fig. 41 Cool-down time temperature profiles during shutdown with several insulation thicknesses of aerogel exposed pipeline in seawater.

This figure shows the impacts of several insulation polyurethane aerogel thicknesses on cool-down time through the shut-down of exposed pipeline in seawater. The polyurethane aerogel has extremely low thermal conductivity, allowing it to be the best insulation material to prevent freezing in subsea pipelines. Fig. 42 demonstrates the temperature along the pipelines which have a polyurethane aerogel layer. An insulation layer of 2.54 cm reduces the pipeline's heat loss and thermal equilibrium of crude oil occurs after 22 hours. As more insulation layers are added, increased cool-down time is achieved. The temperature of crude oil for an insulation layer of 6.35 cm does not fall below 10°C after 42 hours.

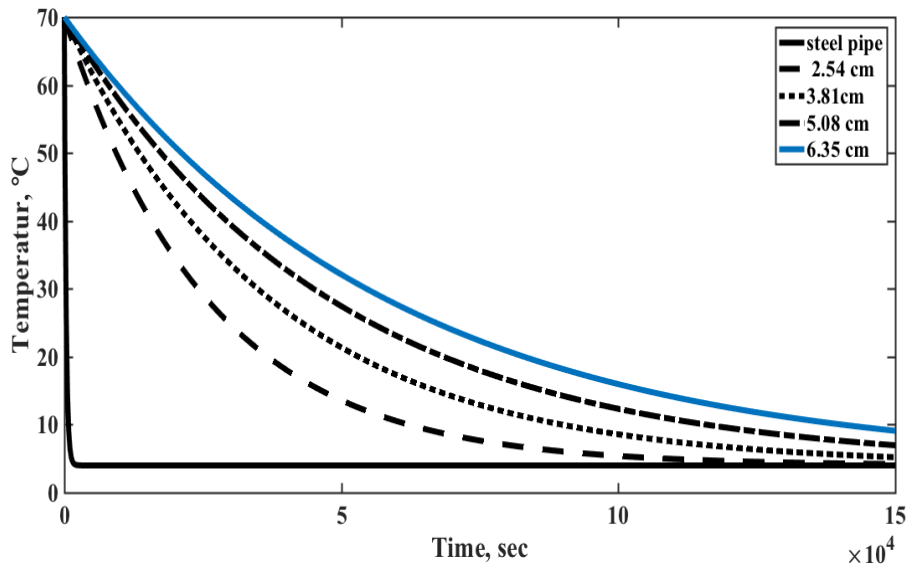


Fig. 42 Cool-down time temperature profiles during shutdown with several insulation thicknesses of polyurethane aerogel exposed pipeline in seawater.

Fig. 43 shows the impacts of several insulation polyurethane foam thicknesses on cool-down time during shut-down for pipeline buried under seawater. The temperature of a pipeline should not reach the critical temperature as that may lead to flow assurance issues such as hydrate formation. The buried steel pipe without insulation reaches thermal equilibrium in 10 hours. Using an insulation layer of 2.54 cm increases the maintenance of the crude oil's thermal energy, as cool-down time is evaluated to reach ambient temperature at 24 hours. For the thickness insulation layer of 6.35cm, the temperature of the crude oil is 7°C at 42 hours.

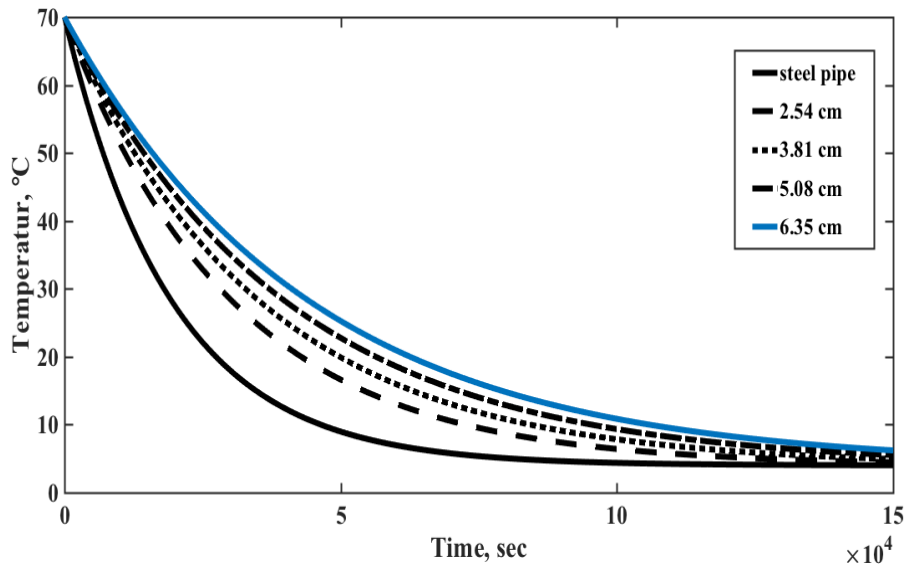


Fig. 43 Cool-down time temperature profiles during shutdown with several insulation thicknesses of polyurethane foam for pipeline buried under seawater.

Fig. 44 shows the impacts of several insulation aerogel thicknesses on cool-down time through shut-down pipeline buried under seawater. For this study, the cool-down time during shut-down of buried pipelines is evaluated. The ability to maintain the thermal energy of crude oil increases with an insulation layer of 2.54 cm, as displayed in the results. Ambient temperature is reached at 37 hours with this layer. The cool-down time increased with increases thickness. The longest cool-down time is for the insulation layer of 6.35 cm, as the temperature does not drop under 12°C within 42 hours.

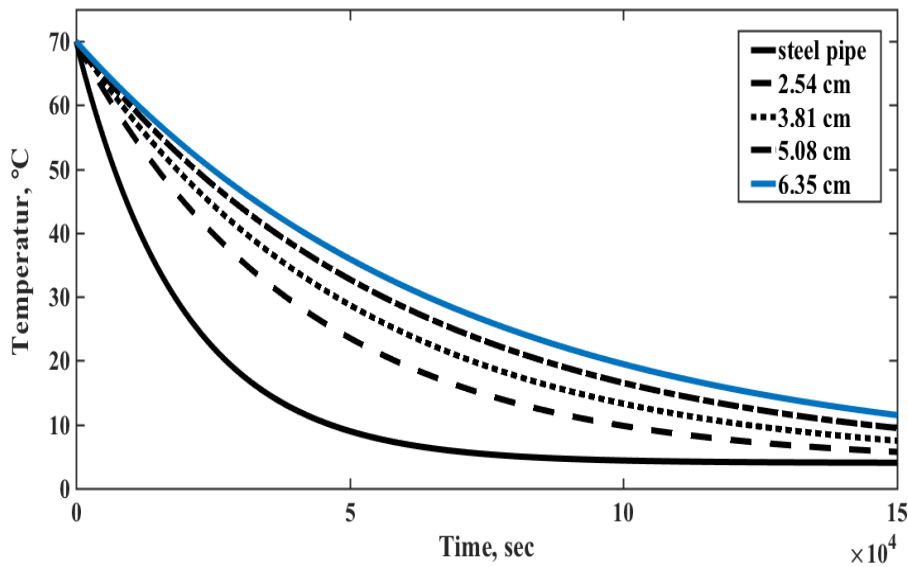


Fig. 44 Cool-down time temperature profiles during shutdown with several insulation thicknesses of aerogel pipeline buried under seawater.

Fig. 45 shows the impacts of several insulation polyurethane aerogel thicknesses on cool-down time through shut-down pipeline buried under seawater. Polyurethane aerogel achieves a long cool-down time, which postpones thermal equilibrium and prevents hydrate formation in subsea pipelines. An insulation layer of 2.54 cm achieves a 25 hour cool-down time. The temperature of crude oil is 10°C higher than the temperature of seawater. The cool-down time increases as thickness increased. For an insulation layer of 6.35 cm the temperature of crude oil is 15°C at 42 hours. Polyurethane aerogel is considered to be the optimal insulation material. It has low thermal conductivity and strong mechanical properties under high pressure, approximately 7.8MPa in the experiment [50].

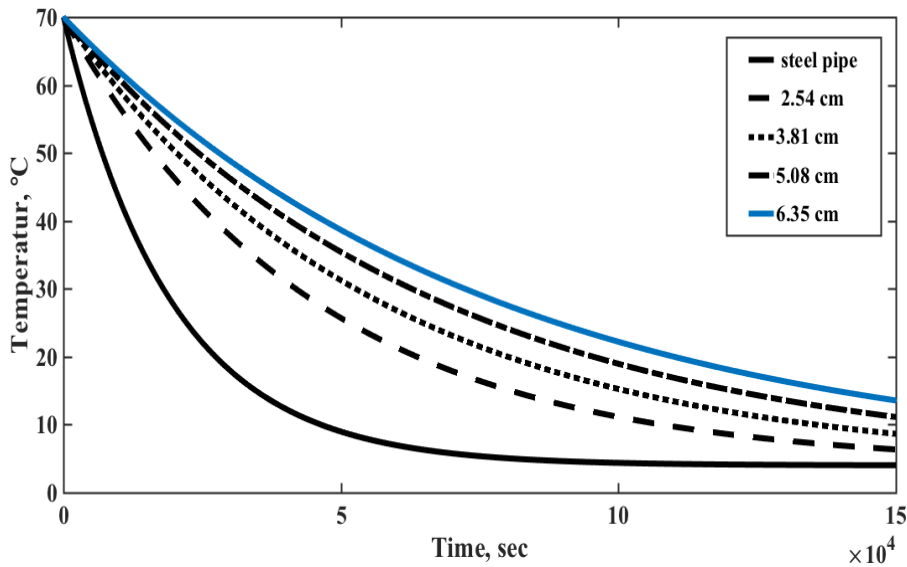


Fig. 45 Cool-down time temperature profiles during shutdown with several insulation thicknesses of polyurethane aerogel for pipeline buried under seawater.

4. ANSYS Fluent (CFD)

Using Fluent CFD for the sample model simulation of insulation pipeline validates results with mathematical modeling for offshore insulation pipelines, as applied above. This modeling focuses on steady state and transient temperature profiles during the start-up of crude oil, and investigates a deviation between both methodologies, as mentioned. The results are obtained from running the calculations.

Fig. 46 shows Fluent CFD runs many times on polyurethane foam coatings, which has the effect of producing optimal insulation thicknesses on the steady state temperature profiles during the start-up of crude oil in an offshore pipeline. Numerical simulation is employed to achieve approximation results, as presented in Fig. 46 with steady state flow temperature profiles simulation using the Fluent CFD energy equation with polyurethane foam layers of four thicknesses, which are (2.54, 3.8, 5.08, and 6.35 cm) respectively. The results show a decrease in deviation for temperature profiles between code and CFD. The T-Test has been evaluated and has a value of less than 1%.

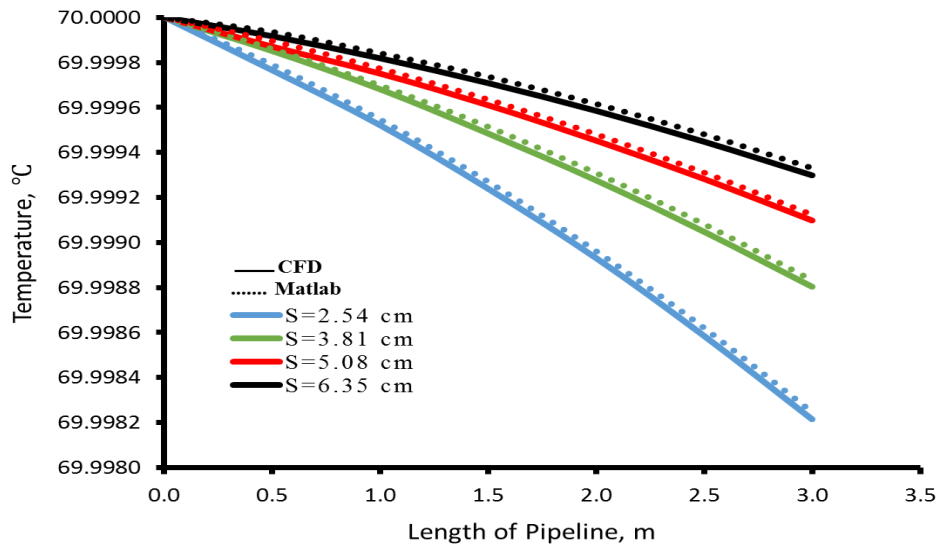


Fig. 46 Validation between CFD and the mathematical model steady state temperature profiles on the length of pipeline subsea with several thicknesses of polyurethane foam.

The Fluent CFD runs to apply a polyurethane foam coating 2.54 cm are considered to be optimal insulation. Fig. 47 presents validation of transient temperature profiles at a location during the start-up of crude oil in an offshore insulated pipeline between Fluent CFD and the mathematical model. For the first case at zero time, the temperature measures 70 °C at the inlet, then slowly is distributed to ambient temperature with mathematical model, but the fast temperature drop with Fluent CFD shows a large temperature deviation in cases 0.5 and 1 second. In case 1.5 seconds, the deviation is small between the mathematical model and Fluent CFD, which explains that the deviation decreases with the locations along the length of the pipeline and with time, as seen in the results.

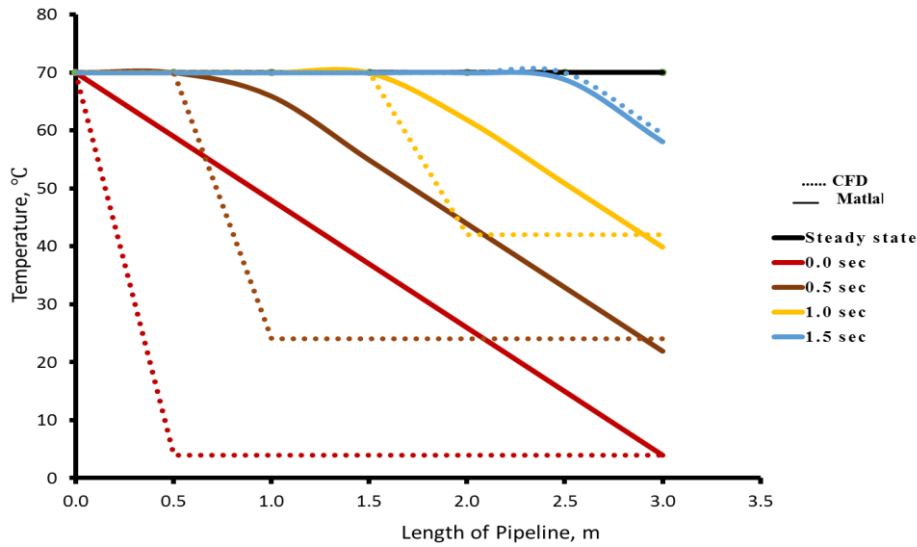


Fig. 47 Validation between CFD and the mathematical model transient temperature profiles on the length of pipeline subsea thickness 2.54 cm of polyurethane foam.

Fig. 48 shows the Fluent CFD runs to apply optimal insulation of aerogel coatings, which focuses on the effect of optimal insulation thicknesses on the steady state temperature profiles during the start-up the crude oil in an offshore pipeline. The aim of numerical simulation is to achieve approximate results, as presented in Fig. 48, the steady state flow temperature profiles simulation using the Fluent CFD energy equation with aerogel layers of four thicknesses, which are (2.54, 3.81, and 5.08 cm), record approximately equal results between Fluent and code, respectively. Therefore, from results achieved, the deviation decreases for temperature profiles through the three layers. However, the layer 6.35 cm is observed to be different. Deviation increases for temperature profiles approximately less than 1% between Fluent CFD and the mathematical model respectively.

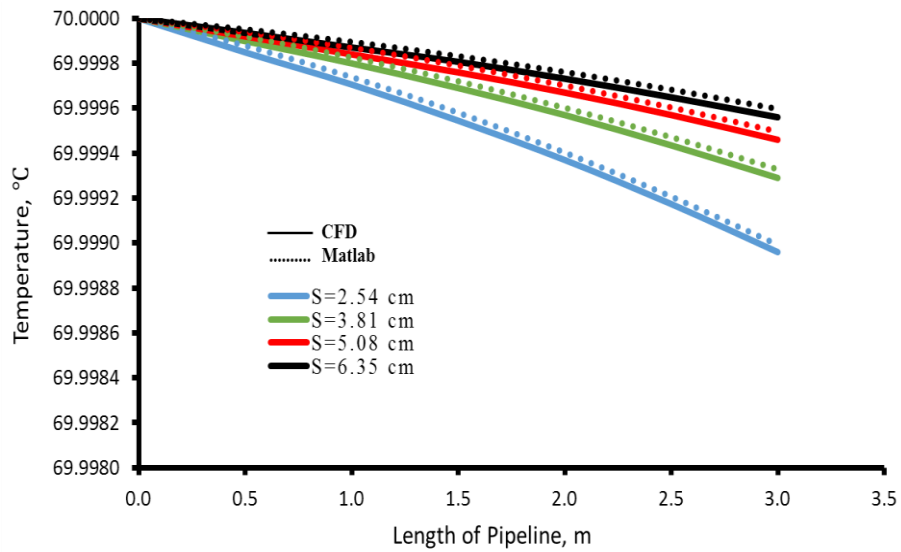


Fig. 48 Validation between CFD and the mathematical model steady state temperature profiles on the length of pipeline subsea with several thicknesses of aerogel.

The Fluent CFD run with the application of aerogel coating 2.54 cm is an optimal insulation. Fig. 49 presents validation for the different transient temperature profiles at locations on the pipeline during the start-up of crude oil in an offshore insulated pipeline for Fluent CFD and the mathematical model. For the first case at zero time, the temperature measures 70°C at the inlet; then slowly is distributed to ambient temperature with code, but a fast temperature drop with Fluent CFD is seen to be a large deviation at the time of cases 0.5, 1 second. The deviation is small between the mathematical model and Fluent CFD at case 1.5 seconds, which explains all the deviation decreases with an increase in the length of pipeline and the time, as seen in the results.

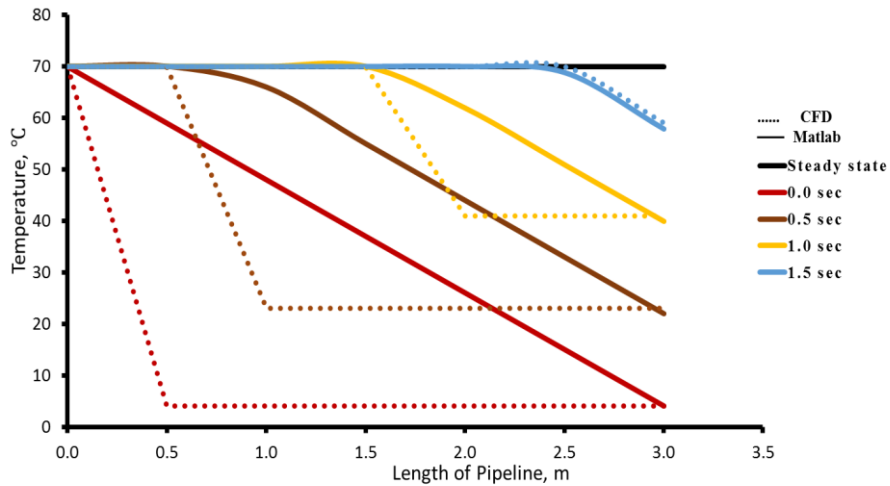


Fig. 49 Validation between CFD and the mathematical model transient temperature profiles on the length of subsea pipeline with thickness 2.54 cm of aerogel.

The Fluent CFD runs apply optimal insulation of aerogel coatings, which focuses on the effect of optimal insulation thicknesses on the steady state temperature profiles during the start-up crude of oil in an offshore pipeline. The aim of the numerical simulation is to evaluate differences in the results presented in Fig. 50 steady state flow temperature profile simulations using the Fluent CFD energy equation. The aerogel layers of four different thicknesses, (2.54, 3.81, 5.08 and 6.35 cm), record different results for Fluent CFD and mathematical model. The results achieved therefore show a deviation decrease for temperature profiles through three layers. However, the layer 6.35 cm is different; therefore, deviation increases for temperature profiles approximately less than 1% between Fluent CFD and mathematical model respectively.

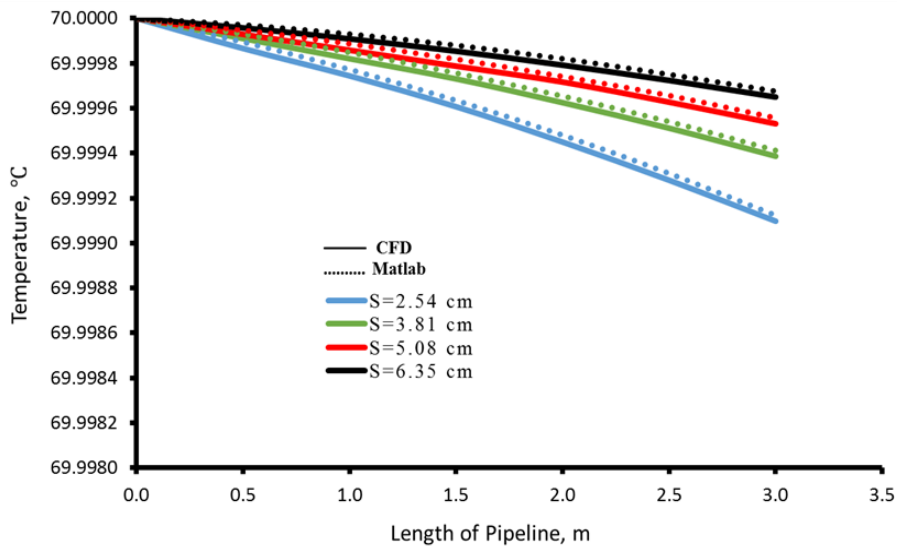


Fig. 50 Validation between CFD and the mathematical model steady state temperature profiles on the length of subsea pipeline with several thicknesses of polyurethane aerogel.

The Fluent CFD runs to apply a polyurethane aerogel coating 2.54 cm are considered to be optimal insulation. Fig. 51 presents validation of transient temperature profiles at a location during the start-up of crude oil in offshore insulated pipeline between Fluent CFD and mathematical model. For the first case at zero time, the temperature measures 70°C at the inlet, then slowly is distributed to the ambient temperature with mathematical model, but the fast temperature drop with Fluent CFD is seen to be a large deviation at the time of cases 0.5 and 1 second. The deviation is small at case 1.5 seconds between the mathematical model and Fluent CFD, which demonstrates that the deviation decreases with an increase in the length of the pipeline and the time, as seen in the results.

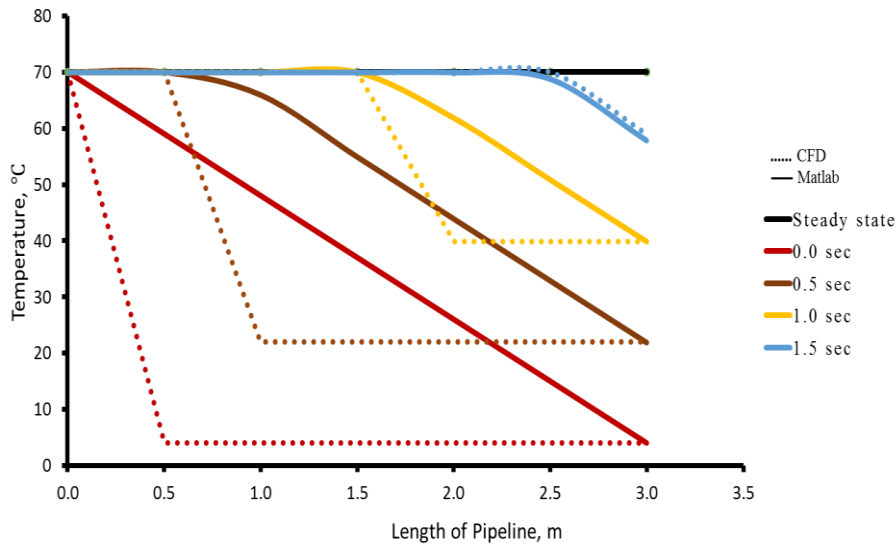
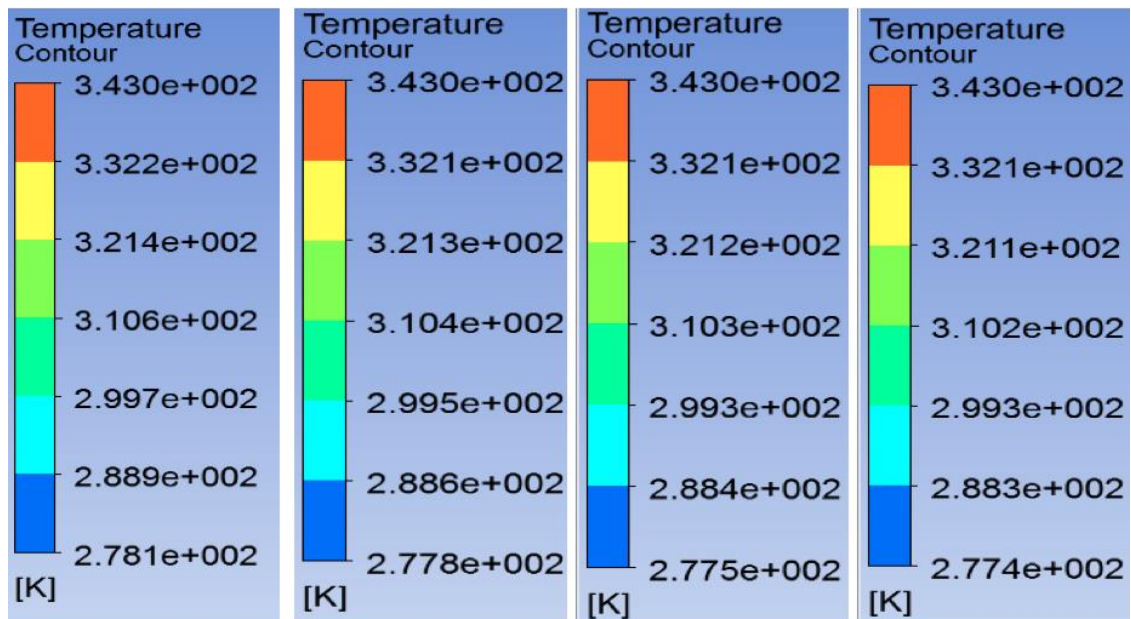


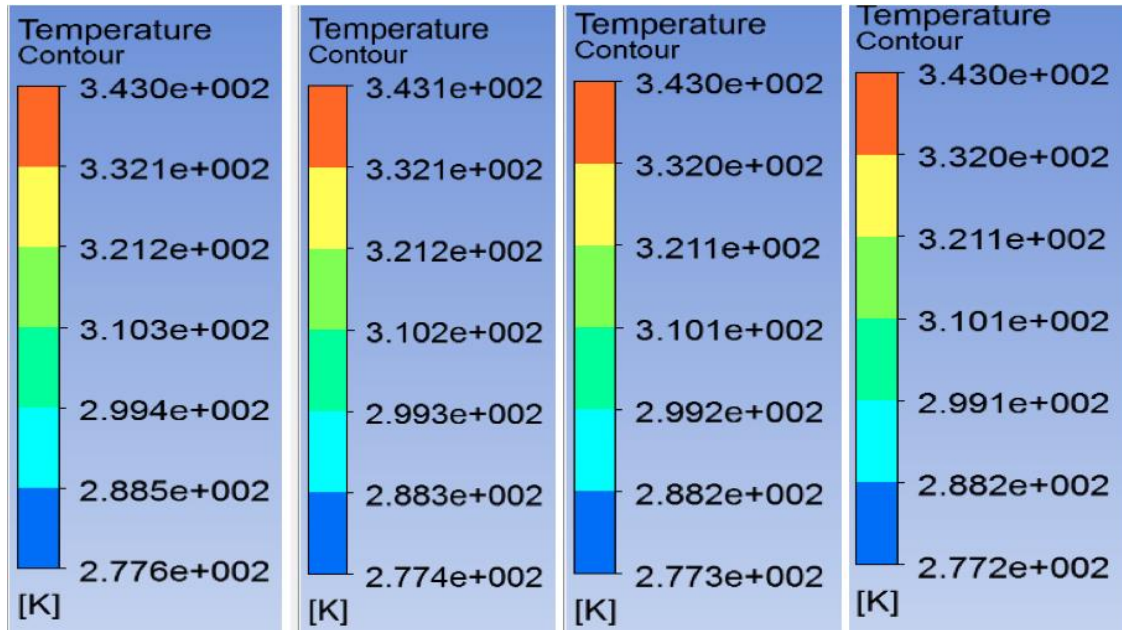
Fig. 51 Validation between CFD and the mathematical model transient temperature profiles on the length of subsea pipeline thickness 2.54 cm of polyurethane aerogel.

Fig. 52 shows the temperature distribution at the diameter of pipeline layers that use several thicknesses insulation of polyurethane foam. Fig. 52 (a, b, c and d) presents the effect of several insulation thicknesses simulation on the temperature distribution through a layer on the radius of the pipeline. The temperature is specified for both the inside of the pipelines and seawater. The heat flow rate is transferred from inside the pipelines to the outside surface of the insulation. This is in terms of the driving force for conduction in each of the two layers' thermal resistance. In addition, there is thermal convective resistance from the outside surface insulation pipelines to the seawater surrounding the insulated pipelines. Note decreases in temperature distribution with increases in the insulation thickness layer on the external walls, as shown in the contours.



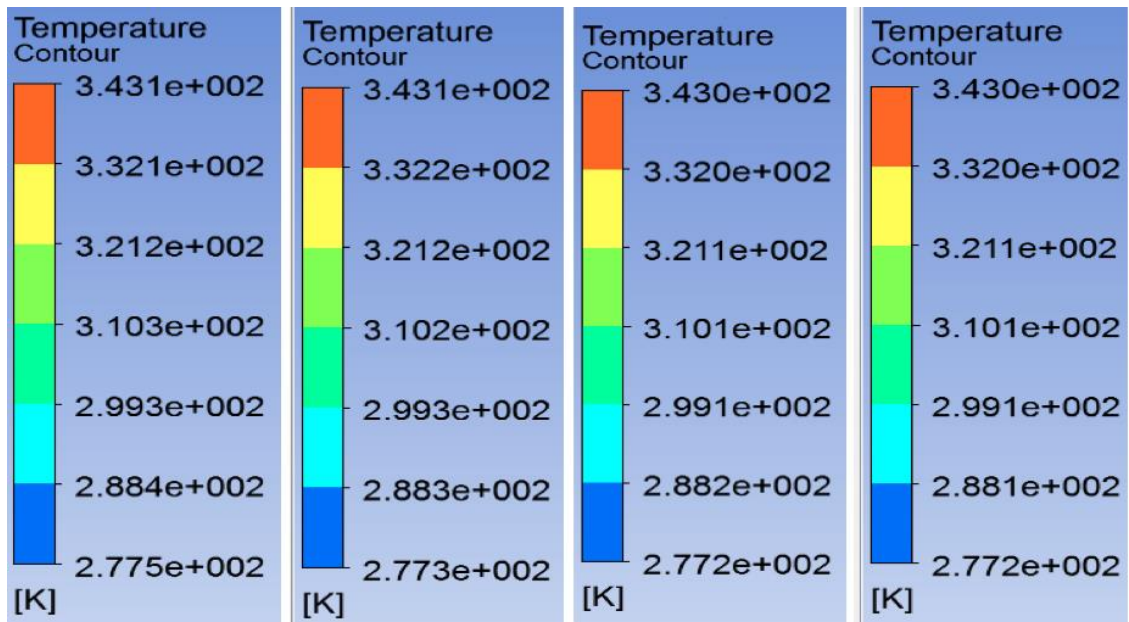
(a) 2.54 cm (b) 3.81 cm (c) 5.08 cm (d) 6.35 cm
 Fig. 52 (a, b, c and d) The effect of several insulation thickness simulations on temperature distribution through layers of polyurethane foam on the radius of the pipeline.

Fig. 53 shows the temperature distribution at the diameter of pipeline layers that use several thicknesses' insulation of aerogel. Fig. 53 (a, b, c and d) presents the effect of several insulation thicknesses simulation on the temperature distribution through a layer on the radius of the pipeline. The overall thermal resistance increases due to the high conduction of thermal resistance of the aerogel insulation material. The temperature distribution is based on the insulation thickness layer and low thermal conductivity of insulation material on the outer walls, as displayed in Fig. 53. For example, aerogel decreases the temperature more than the polyurethane foam dose.



(a) 2.54 cm (b) 3.81cm (c) 5.08 cm (d) 6.35 cm
 Fig. 53 (a, b, c and d) The effect of several insulation thickness simulations on temperature distribution layers of aerogel on the radius of the pipeline.

Fig. 54 shows the temperature distribution at the diameter of pipeline layers that use several thicknesses insulation of polyurethane aerogel. Fig. 54(a, b, c and d) presents the effect of several insulation thicknesses simulation on the temperature distribution through a layer on the radius of the pipeline. The heat flow rate reduces from the inside to the outside of pipelines due to the low overall heat transfer coefficient. The polyurethane aerogel material is a better insulation material than polyurethane foam and aerogel. This is due to the temperature distribution and low temperature on the outside insulation wall as displayed in Fig. 54.



(a) 2.54 cm (b) 3.81 cm (c) 5.08 cm (d) 6.35 cm

Fig. 54 (a, b, c and d) The effect of several insulation thickness simulations on temperature distribution layers of polyurethane aerogel on the radius of the pipeline.

CHAPTER FIVE: CONCLUSIONS AND FUTUER WORK

This research focuses on flow assurance and overcoming the issue of heat loss in subsea pipelines that are used for the transportation of crude oil and gas. The thesis develops the model with optimal thermal insulation material, which keeps thermal energy in the flowline during start-up and shutdown of subsea pipelines. Modeling is used to control temperature distribution for the crude oil and prevent the formation of hydrates and wax asphaltic caused by its transportation in subsea pipelines. This research considers the determination of the effects produced with several thicknesses of insulation and several insulation materials for steady state and transient flow, using temperature profiles during the start-up of crude oil in subsea pipelines. The results shown in the study for polyurethane foam and aerogel do not meet the designated standard layer of 2.54 cm at the end of the pipeline, but the standard layer with polyurethane aerogel is measured at 67.3°C, as needed. This research considers the cool-down time during the shutdown of the flowline for exposed pipeline in seawater and pipeline buried under seawater. The results presented for pipeline exposed to seawater with the standard layer of steel pipe is at less than an hour, for polyurethane foam is recorded at approximately 13 hours, for aerogel recorded at more than 22 hours and for polyurethane aerogel recorded at approximately 27 hours. However, the result for the pipeline buried under seawater with a standard layer of steel pipe increases to 10 hours, for polyurethane foam increases to 26 hours, for aerogel increases to 37 hours and for polyurethane aerogel achieves more than 42 hours. Validation between mathematical model and ANSYS Fluent CFD was conducted. The validation results achieved are approximate. In this research, polyurethane aerogel is recommended as the optimal insulation material, as demonstrated in the results. It has a low thermal conductivity of approximately 0.017W/m K and strong mechanical

properties under high pressure of approximately 7.8MPa, and has no breakage during the experiments. Polyurethane aerogel will work in extremely deep ocean water.

Future Work

The research indicates a few suggestions to be considered for further work:

Experiments are recommended to validate the results in this research, using a sample of pipeline of three meters and a standard layer 2.54 cm (1 in) thick of polyurethane aerogel, which is the optimal insulation material in this research. A thermocouple can measure the temperature on location in a steady state or for a transient state in the pipeline.

This research only uses single phase flow; therefore, for further work it is recommended to use multiphase flow. In this case, many tools may be used to advance the study. For example, a camera could follow the flow when fully developed in the pipeline. Also, studies could include parameters such as pressure, velocity, fraction and viscosity of crude oil in a pipeline, that focus on the effects of low temperature and viscosity of crude oil on pump power consumption.

REFERENCES

- [1] C. An and J. Su, “Lumped Models for Transient Thermal Analysis of Multilayered Composite Pipeline with Active Heating”, *Applied Thermal Engineering*, vol. 87, pp. 749–759, 2015.
- [2] C. Valle-Molina, J. L. Alamilla, J. Sanchez-Moreno, S. S. Najjar, and N. P. Lopez-Acosta, “Reliability Functions for Buried Submarine Pipelines in Clay Subjected to Upheaval Buckling”, *Applied Ocean Research*, vol. 48, pp. 308–321, 2014.
- [3] G. Zheng and D. Cai, “An Update on Heat Transfer in a Porous Insulation Medium in a Subsea Bundled Pipeline”, *Journal of Energy Resources Technology*, vol. 123, pp. 285-290, 2001.
- [4] F. Grosjean, N. Bouchonneau, D. Choqueuse, and V. Sauvart-Moynot, “Comprehensive Analyses of Syntactic Foam Behaviour in Deepwater Environment”, *Journal. Material Science*, vol. 44, no. 6, pp. 1462–1468, 2009.
- [5] D.P.S Abam V. Adukwu, “Spreadsheet Modeling of Thermal Insulation in Deep Water Flow Lines”, *Global Journal. Research in Engineering*, vol. 11, pp. 1, 2011.
- [6] A. Nazari, P. Rajeev, and J. G. Sanjayan, “Modelling of Upheaval Buckling of Offshore Pipeline Buried in Clay soil Using Genetic Programming”, *Engineering. Structures*, vol. 101, pp. 306–317, 2015.
- [7] D. J. White, A. J. Barefoot, and M. D. Bolton, “Centrifuge Modelling of Upheaval Buckling in Sand”, *International Journal. Physical Model Geotechn*, vol. 2, pp. 19-28, Sep. 2000.
- [8] J. Schupp, B. W. Byrne, N. Eacott, C. M. Martin, J. Oliphant, A. Maconochie, and D. Cathie. “OMAE2006-92542 Pipeline Unburial Behavior in Loose Sand”, *Conference, Offshore Mechanics and Arctic Engineering*, 2006.
- [9] N. I. Thusyanthan, S. Arasu, M. D. Bolton, and P. Allan, “Upheaval Buckling Resistance of Pipelines Buried in Clayey Backfill”, *Paper, ISOPE-2008-TPC-*

499, 2008.

- [10] A. Ivanovic, J. Oliphant, “Uplift Mobilisation Resistance of Subsea Pipelines in Loose Sand”, *Geotechnique Letters*, vol. 4, Iss. 3, pp. 217-222, July 2014.
- [11] W. Pao, “Optimum Thermal Insulation Design for Subsea Pipeline Flow Assurance”, *Petroleum Engineering*, September, 2016.
- [12] O. Wilfred and D. Appah, “Analyzing Thermal Insulation for Effective Hydrate Prevention in Conceptual Subsea Pipeline Design”, vol. 5, pp. 4, 2015.
- [13] T. Lu and K. Wang, “Numerical Analysis of the Heat Transfer Associated with Freezing / Solidifying Phase Changes for a Pipeline Filled with Crude Oil in Soil Saturated with Water During Pipeline Shutdown in Winter”, *Journal of Petroleum Science and Engineering*, vol. 62, pp. 52–58, 2008.
- [14] A. C. Palmer and R. A. King, “Subsea Pipeline Engineering”, (2 Ed) Ch. 10 Strength, Pennwell Books, ISBN: 978-1-59370-133-8, pp. 327-360, 2004.
- [15] A. J. Brennan, M. Ghahremani, and M. J. Brown, “Strength Reduction for Upheaval Buckling of Buried Pipes in Blocky Clay Back Fill”, *Ocean Engineering*, vol. 130, pp. 210–217, 2017.
- [16] L. Wang, R. Shi, F. Yuan, Z. Guo, and L. Yu, “Global Buckling of Pipelines in the Vertical Plane with a Soft Seabed”, *Applied. Ocean Research*, vol. 33, pp. 130–136, 2011.
- [17] C. Y. Cheuk, W. A. Take, M. D. Bolton, and J. R. M. S. Oliveira, “Soil Restraint on Buckling Oil and Gas Pipelines Buried in Lumpy Clay Fill”, *Engineering Structures*, vol. 29, pp. 973–982, 2007.
- [18] A. Young, R. Osborne, and I. Frazer, “Utilizing Thermal Properties of Seabed Soils as Cost-Effective Insulation for Subsea Flowlines”, *Offshore Technology. Conferance*, vol. 1, pp. 1–6, 2001.
- [19] Y. Bai and J. M. Niedzwecki, “Modeling Deepwater Seabed Steady-State Thermal Fields Around Buried Pipeline Including Trenching and Backfill Effects”, *Computers Geotechnics*, vol. 61, pp. 221–229, 2014.

- [20] Y. Bai, Q. Bai, “Subsea Pipelines and Risers”, Part III, Flow Assurance, Ch. 19 Heat Transfer and Thermal Insulation, pp. 317-336, 2005.
- [21] S. Chakraborty, V. Talimi, Y. Muzychka, G. Piercey, and R. Mcaffee, “Design of Experiment and Validation of Model for Offshore Buried Pipeline Thermal Analysis”, International Pipeline Conference, pp. 1–9, 2017.
- [22] H. Maleki, L. Durães, and A. Portugal, “Synthesis of Lightweight Polymer-Reinforced Silica Aerogels with Improved Mechanical and Thermal Insulation Properties for Space Applications”, Microporous Mesoporous Material, vol. 197, pp. 116–129, 2014.
- [23] J. C. H. Wong, H. Kaymak, P. Tingaut, S. Brunner, and M. M. Koebel, “Mechanical and Thermal Properties of Nanofibrillated Cellulose Reinforced Silica Aerogel Composites”, Microporous Mesoporous Mater, vol. 217, pp. 150–158, 2015.
- [24] N. Diascorn, S. Calas, H. Sallée, P. Achard, and A. Rigacci, “Polyurethane Aerogels Synthesis for Thermal Insulation Textural, Thermal and Mechanical Properties”, J. Supercrit Fluids, vol. 106, pp. 76-84, 2015.
- [25] M. Karkri, M. Lachheb, Z. Nogellova, B. Boh, B. Sumiga, M. A. Almaadeed, A. Feth, I. Krupa, “Thermal Properties of Phase Change Materials Based on High-Density Polyethylene Filled with Micro Encapsulated Paraffin Wax for Thermal Energy Storage”, Energy Build, vol. 88, pp. 144–152, 2015.
- [26] M. Lachheb, M. Karkri, and S. Ben Nasrallah, “Development and Thermal Characterization of an Innovative Gypsum-Based Composite Incorporating Phase Change Material as Building Energy Storage System”, Energy Build, vol. 107, pp. 93–102, 2015.
- [27] Y. Wu and T. Wang, “Hydrated Salts/Expanded Graphite Composite with High Thermal Conductivity as a Shape-Stabilized Phase Change Material for Thermal Energy Storage”, Energy Conversion Managment, vol. 101, pp. 164–171, 2015.
- [28] Yong Bai, Qiang Bai (Eds) Subsea Pipelines and Risers, Part III, Flow Assurance, Ch. 20 Haydrates, pp. 358-381, 2005.

- [29] R. Gudimetla, A. Carrol, K. Havre, C. Christian and J. Canon, “Gulf of Mexico Field of the Future Subsea Flow Assurance”, Offshore Technology Conference, Houston, Texas, USA, 2006.
- [30] D. Janoff, N. Mckie, and J. Davalath, “Prediction of Cool Down Times and Designing of Insulation for Subsea Production Equipment”, Offshore Technology Conference OTC 16507, pp. 1–6, 2004.
- [31] H. J. Huo, R. H. Wang, H. J. Ni, and Y. L. Liu, “An Experimental Study on the Synergetic Effects of Kinetic and Thermodynamic Gas Hydrate Inhibitors”, *Petroleum Sciences Technology*, vol. 32, pp. 1940–1947, 2014.
- [32] A.C. Palmer, R.A King, *Subsea Pipeline Engineering*, Ch. 9 Pipeline Hydraulics pp. 305-326, Penn Well Book, 2008.
- [33] G. S. Dulikravich, “IHTC14-22462 Temperature Field Prediction of a Multilayered Composite Pipeline”, pp. 1–10, 2010.
- [34] R. Hoffmann, L. Amundsen and R. Schuller, “Online Monitoring of Wax Deposition in Subsea Pipelines”, *Measurement Sciences Technology*, vol. 22, 75701, 2011.
- [35] S. Jung and P. Kang, “An Experimental Study on the Effects of Internal Tubular Coatings on Mitigating Wax Deposition in Offshore Oil Production”. *J. Korean Soc. Maritime Engg*, vol. 38, pp. 1333–1339, 2014.
- [36] S. Kiil, “Model-Based Analysis of Thermal Insulation Coatings”, *J. Coatings Technology*, vol. 11, pp. 495–507, July 2014.
- [37] S. Corraera, A Fasano, L. Fusi and D. Merino, “Calculating Deposit Formation in the Pipelining of Waxy Crude Oils”, *Applied Mechanics*, pp. 149–165, 2007.
- [38] B. A. I. Chengyu and Z. Jinjun, “New Method to Determine the Strength of Wax Deposits in Field Pipelines”, *Advances in Petroleum Exploration and Development*, vol. 10, pp. 31–36, 2015.
- [39] Z. Tian, W. Jin, L. Wang and Z. Jin, “The Study of Temperature Profile Inside Wax Deposition Layer of Waxy Crude Oil in Pipeline”, *Frontiers in Heat and*

ass Transfer, vol. 5, 2014.

- [40] Yong Bai, Qiang Bai (Eds) Subsea Pipelines and Risers, Part III, Flow Assurance, Ch. 21 Wax and Asphaltenes, pp. 383-398, 2005.
- [41] R. C. Saramento, G. A. S. Ribbe, and L. F. A. Azevedo, “Wax Blockage Removal by Inductive Heating of Subsea Pipelines”, Heat Transf Engineering, vol. 25, pp. 2–12, 2004.
- [42] M. Halstensen, B. K. Arvoh, L. Amundsen, and R. Hoffmann, “Online Estimation of Wax Deposition Thickness in Single-Phase Subsea Pipelines Based on Acoustic Chemometrics A Feasibility Study”, Fuel, vol. 105, pp. 718–727, 2013.
- [43] M. Parsazaded and X. Duan, “Thermal Insulation with Latent Energy Storage for Flow Assurance in Subsea Pipelines”, International Conference on Ocean, Offshore and Arctic Engineering, St. John's, Newfoundland, Canada, OMAE 2015-41285.
- [44] S. Denniel, S. Hall, H. De-Naurois, T. Parenteau, F. Gooris, Mechanical and Thermal Qualification of an Electrically Heated Pipe-in-Pipe (EH-PIP) and Application to Subsea Field Development, AMSE, International Confernce on Ocean Offshore and Arctic Engineering, PP. 375-385, 2010.
- [45] X. Duan, “Phase Change Heat Transfer and Materials for Thermal Management in Energy and Power Systems”, International Workshop on Heat Transfer Advances for Energy Conservation and Pollution Conttrol, IWHT 2015-1143.
- [46] Q. Bai and Y. Bai, “Hydraulic and Thermal Analysis of Subsea Pipelines Subsea Pipeline Design, Analysis and Installation”, (1thEd), USA, ISBN: 978-0-12-3868886, 2014.
- [47] A. Y. Cengel, “Fundamentals of Engineering Heat and Mass Transfer”, A Practical Approach, 2nd Ed, New Age International Publishers, 2006.
- [48] Bergman, Theodore L., and Frank P. Incropera, Fundamentals of Heat and Mass Transfer (7thEd), John Wiley and Sons, 2011.

- [49] Y. Başıođul and A. Keęebaş, “Economic and Environmental Impacts of Insulation in District Heating Pipelines”, *Energy*, vol. 36, pp. 6156–6164, 2011.
- [50] T. Galta, “Pipelines Suffering Wax Deposition”, Master Thesis, Norwegian University of Science and Technology, 2014.
- [51] D. W. Mackowski, “Conduction Heat Transfer”, Mechanical Engineering Department, Auburn University, Notes for MECH 7210, 2011.
- [52] S. Duplenskiy, “Protection of Subsea Pipelines Against Ice Ridge Gouging in Conditions of Substantial Surface Ice”, Univerasity of Stavanger, Faculty of Science and Technology, Master Thesis, 2012.
- [53] Yong Bai, Qiang Bai (Eds) *Subsea Pipelines and Risers, Part II, Pipeline Design*, Ch. 13 Pipe-in-Pipe and Bundle Systems, pp. 196-218, 2005.
- [54] B. Guo, S. Duan, and A. Ghalambor, “A Simple Model for Predicting Heat Loss and Temperature Profiles in Insulated Pipelines”, *Society of Petroleum Engineers, Production and Operations*, vol. 21, pp. 107–113, 2006.
- [55] A. Bahadovi, “Thermal Insulation for Offshore Installations in Deep Water. Handbook”, Chapter Five, ISBN 978-0-12-800010-6, 2015.
- [56] S. Sadafule and K. D. Patil, “Study on Effect of Insulation Design on Thermal-Hydraulic Analsis an Important Aspect in Subsea Pipeline Designing”, *Journal of Petroleum Engineering and Technology*, vol. 4, pp. 2231-1785, 2014.
- [57] D. Sofialidis, “Turbulenece Modeling, Heat Transfer and Transient Calculations”, *Introduction to ANSYS Fluent*, University of Ljubljana, Faculty of Mechanical Engineering, Slovenia, 14.5 Release, 2013.
- [58] D. Sofialidis, “Express Introductory Training in ANSYS Fluent Turbulence Modeling , Heat Transfer & Transient Calculations Turbulence Modeling, Heat Transfer & Introduction to ANSYS Fluent”, pp. 1–72, 2013.
- [59] F. P. Incropera, D. P. DeWitt, *Fundamentals of Heat and Mass Transfer* (6th Ed.), New York, Wiley, 2007.